Journal of Medicinal Chemistry

Article

Comprehensive Structure Activity Relationship of Triantennary *N*-Acetylgalactosamine Conjugated Antisense Oligonucleotides for Targeted Delivery to Hepatocytes

Thazha P. Prakash, Jinghua Yu, Michael T. Migawa, Garth A. Kinberger, W. Brad Wan, Michael E Østergaard, Recaldo L Carty, Guillermo Vasquez, Audrey Low, Alfred Chappell, Karsten Schmidt, Mariam Aghajan, Jeff Crosby, Heather M. Murray, Sheri L. Booten, Jill Hsiao, Armand Soriano, Todd Machemer, Patrick Cauntay, Sebastien A. Burel, Susan F. Murray, Hans J. Gaus, Mark J. Graham, Eric E. Swayze, and Punit P Seth

J. Med. Chem., **Just Accepted Manuscript** • DOI: 10.1021/acs.jmedchem.5b01948 • Publication Date (Web): 25 Feb 2016

Just Accepted

ACS Publications

Journal of Medicinal Chemistry is published by the American Chemical Society. 1155 Sixteenth Street N.W., Washington, DC 20036

Comprehensive Structure Activity Relationship of Triantennary *N*-Acetylgalactosamine Conjugated Antisense Oligonucleotides for Targeted Delivery to Hepatocytes

Thazha P. Prakash*, Jinghua Yu, Michael T. Migawa, Garth A. Kinberger, W. Brad Wan, Michael E. Østergaard, Recaldo L. Carty, Guillermo Vasquez, Audrey Low, Alfred Chappell, Karsten Schmidt, Mariam Aghajan, Jeff Crosby, Heather M. Murray, Sheri L. Booten, Jill Hsiao, Armand Soriano, Todd Machemer, Patrick Cauntay, Sebastien A. Burel, Susan F. Murray, Hans Gaus, Mark J. Graham, Eric E. Swayze and Punit P. Seth

IONIS Pharmaceuticals Inc., 2855 Gazelle Court, Carlsbad, CA 92010

*tprakash@ionisph.com, Tel 760-603-2590

ABSTRACT

The comprehensive structure-activity relationships of triantennary GalNAc conjugated ASOs for enhancing potency *via* ASGR mediated delivery to hepatocytes is reported. Seventeen GalNAc clusters were assembled from six distinct scaffolds and attached to ASOs. The resulting ASO conjugates were evaluated in ASGR binding assays, in primary hepatocytes and in mice. Five structurally distinct GalNAc clusters were chosen for more extensive evaluation using ASOs targeting SRB-1, A1AT, FXI, TTR and ApoC III mRNAs. GalNAc ASO conjugates exhibited excellent potencies (ED_{50} 0.5–2 mg/kg) for reducing the targeted mRNAs and proteins. This work culminated in the identification of a simplified tris-based GalNAc cluster (THA-GN3), which can be efficiently assembled using readily available starting materials and conjugated to ASOs using a solution phase conjugation strategy. GalNAc-ASO conjugates thus represent a viable approach for enhancing potency of ASO drugs in the clinic without adding significant complexity or cost to existing protocols for manufacturing oligonucleotide drugs

INTRODUCTION

Antisense oligonucleotides bind their cognate mRNA and modulate its function to yield a pharmacological response.[1] A second generation gapmer ASO typically consists of a central gap region of 8-14 DNA nucleotides adjoined on either end with 2'-*O*-methoxyethyl RNA [2] (MOE, Figure 1) nucleotides and phosphorothioate (PS) backbone chemistry.[3] Kynamro, a second generation ASO targeting Apolipoprotein B-100 mRNA, was recently approved by the FDA for the treatment of homozygous familial hypercholesterolemia.[4] Currently, there are more than 35 ASOs advancing in clinic for the treatment of cardio-vascular, diabetes, cancer and several rare and orphan disease indications.[5,6] Significant number of these ASOs target mRNAs expressed primarily in hepatocytes in the liver.[6,7] Therefore, delivery approaches which enhance ASO potency for suppressing gene targets of therapeutic interest expressed in hepatocytes are beneficial.

The ASGR (asialoglycoprotein receptor)[8] is abundantly expressed on hepatocytes (~500,000 copies/cell)[9,10] and it clears glycoproteins from serum by receptor mediated endocytosis.[11] The functional ASGR exhibits high affinity for *N*-acetyl galactosamine (GalNAc) terminated oligosaccharides and is conserved across all mammals.[12] The receptor binding is mediated by calcium[13] and is sensitive to pH. The receptor ligand complex dissociates in acidic pH within endosomes and receptor recycle back to the cell surface.[14] ASGR has been exploited for the targeted delivery of modified lipoprotein particles[15], genes[16], chemically modified oligonucleotides[17,18] siRNA[19,20] and microRNA antagonists[21] to hepatocytes in rodents. Additionally, in an early stage human trials, siRNA conjugates targeting transthyretin (TTR) mRNA, have exhibited good activity for reducing TTR protein in blood.[22]

We recently reported that targeted delivery of ASOs to hepatocytes using a previously reported tri-antennary GalNAc cluster attached to the 3'-end of an ASO improved ASO activity 7-10 fold in rodents.[23] Our initial studies were carried out using the Tris-GN3 cluster (Figure 2) which has been successfully used for evaluation of siRNA GalNAc conjugates in rodents and in humans and is attached to the 3'-end of the oligonucleotide.[20] The 3'-Tris-GN3 oligonucleotide conjugates were synthesized by pre-loading an appropriately modified Tris-GN3 cluster onto solid-support followed by automated oligonucleotide synthesis.[19] While this approach was efficient, it was not amenable for rapid evaluation of multiple GalNAc clusters. Furthermore, the synthesis of the Tris-GN3 cluster can be cumbersome as additional steps are required for attaching the propanediamine adaptor which links the GalNAc-acid moiety to the Tris-tricarboxylic acid scaffold.

To address these issues, we showed that attaching the Tris-GN3 cluster to the 5'-end of ASOs can be carried out efficiently using a solution-phase conjugation reaction and that the 5'-Tris-GN3 ASO was slightly more active than the corresponding 3'-Tris-GN3 ASO conjugate in mice.[24] To determine if the structure of the Tris-GN3 cluster can be further simplified while retaining ASGR binding and in vivo activity, we carried out a systematic structure activity relationship (SAR) study to identify the optimal structural requirements of triantennary GalNAc conjugates for enhancing ASO delivery to hepatocytes. As part of this effort, we examined the ASGR binding, *in vitro* and *in vivo* activity of ASOs conjugated to several GalNAc clusters with different linking scaffolds and tethers. In addition, we also examined the effect of ASO backbone chemistry and the linker moiety on the potency of GalNAc conjugated ASOs. After initial profiling of the GalNAc conjugates, five clusters were selected for more extensive evaluation using multiple ASO sequences for potency and toxicity assessments. This effort led to the

identification of several triantennary GalNAc clusters with simplified structures which are easier to synthesize and enhance ASO potency >10-fold in mouse models. Our work represents a comprehensive study on the structure activity relationships of triantennary GalNAc conjugated ASOs for enhancing potency by targeted delivery to hepatocytes in animals.

RESULTS AND DISCUSSION

Previous studies have described the SAR of multivalent galactose and GalNAc (Figure 1) clusters derived from amino acid and dendrimer based scaffolds for ASGR binding.[25-28] Affinity of the sugar clusters for the ASGR was dependent on the nature of the sugar (GalNAc>galactose),[12] number of sugars (four=three>two>one),[29-31] and on the length and hydrophobicity of the spacer between the sugar moieties and the branching point of the dendrites.[25, 26] A galactose cluster with a 20 Å spacer exhibited 2000-fold higher affinity for the ASGR than galactose clusters lacking the spacer.[26] These data suggested that the spatial orientation of the sugars within the cluster was important for optimal ASGR binding. To determine if these structural requirements were also valid for triantennary GalNAc clusters attached to single stranded chemically modified ASOs, we examined GalNAc clusters assembled on six distinct scaffolds. These scaffolds were abbreviated as Tris, Triacid, Lys-Lys, Lys-Gly, Trebler and Hydroxyprolinol (Figure 2) based on the building blocks used to assemble the clusters. For several of the scaffolds, we also varied the length and hydrophobicity of the linkers used to attach the GalNAc sugars to the branching points on the scaffold.

Synthesis of GalNAc clusters. The general synthetic protocols for the preparation of the Tris, Triacid, Lys-Lys, and hydroxyprolinol type GalNAc clusters (**1-11**, Scheme 1) have been described previously and additional details are provided in the supporting information.[23,26,32-34]

Synthesis of the simplified Tris-based cluster THA-GN3-Pfp **3** is shown in Scheme 2. The *N*-acetylgalactosamine building block **12** (Scheme 2) was synthesized by glycosylation of known[35] oxazoline **13** with benzyl (6-hydroxyhexyl)carbamate **14** in presence of trimethylsilyl trifluoromethanesulfonate (TMSOTf). The previously reported Tris based triantennary core-unit **15** (Scheme 2) [36] was functionalized by mono-benzyl protected glutaric acid **16** (Supporting Information) under standard amino acid coupling conditions followed by treatment with trifluoroacetic acid (TFA) to deprotect *tert*-butyl ester yielded tris acid **17** (80%). The tris acid **17** was further reacted with pentafluorophenol-trifluoracetate (Pfp-TFA) in the presence of *N*,*N*-diisopropylethylamine resulting in clean conversion to the corresponding Pfp ester **18** (83%).[37] The tris Pfp ester **18** was reacted with GalNAc analog **12** in presence of palladium hydroxide in THF under an atmosphere of hydrogen to yield THA-GN3 glutaric acid analog **19** (76%). The THA-GN3 glutaric acid analog **19** was conveniently converted to its Pfp ester **3** by reacting with Pfp-TFA in the presence of triethylamine in high yield.

Synthesis of GalNAc-ASO conjugates. The general protocol for synthesis of the GalNAc cluster ASO conjugates is depicted in Scheme 1.[24] In brief, a solution of 10-12 mM 5'-hexylamino ASO **20** (Scheme 1) in sodium tetraborate buffer (pH 8.5) was added to a solution of triantennary GalNAc Pfp esters (2-3 mole equivalents, 30-40 mM) in DMSO and the resulting solution was stirred at room temperature for 3 h. The 5'-hexylamino ASO **20** was completely consumed in 3 h as seen by LC MS analysis. The *O*-acetyl groups from the GalNAc sugar were removed by treating with aqueous concentrated ammonia (28-30 wt%) for 2-3 h followed by HPLC purification to provide the triantennary GalNAc conjugated ASOs.

The synthesis of Trebler based GalNAc clusters (Figure 2, PGN3, Pip-PGN3) was accomplished according to reported procedures using GalNAc phosphoramidites **21** and **22**

(Figure 3, Supporting Information).[24] Hydroxyprolinol based GalNAc cluster conjugated ASOs (Figure 2, 3'-HP-H-GN3, 3'-HP-DGN3, 3'-HP-HAH-GN3) were synthesized on a DNA synthesizer using the phosphoramidites **23-24** (Scheme 3) and **25** (Figure 3). Tetra acetyl-GalNAc analogs **26** and **27** (Scheme 3, Supporting Information) were conveniently coupled to 6-*O*-DMT-hydroxyprolinol[23,34] **28** (Scheme 3) under peptide coupling conditions to yield compounds **29-30** (Scheme 3, Supporting Information). Compounds **29-30** were phosphitylated to provide phosphoramidites **23-24** (Scheme 3, Supporting Information).

The phosphoramidites **23-25** were sequentially coupled three times on a UnyLinker™ solid support to create the hydroxyprolinol-based trivalent GalNAc clusters (Figure 2). Subsequently, DNA or MOE nucleoside phosphoramidites were coupled to the solid support to assemble the ASO using standard oligonucleotide synthesis protocols.[38] Interestingly, the opposite configuration where the hydroxyprolinol GalNAc phosphoramidites were coupled to the 5'-end of the ASO on solid support was not successful due to poor coupling efficiencies. After completion of the synthesis, the solid support was treated with 50% triethylamine in acetonitrile at room temperature to remove cyanoethyl group from internucleosidic linkages. Next, the solid support bearing the ASO GalNAc cluster conjugate was treated with aqueous ammonia to release the 3'-hydroxyprolinol based GalNAc ASO conjugate from the solid support and to remove the protecting groups from exocyclic amino groups of the nucleobases. ASO conjugates were purified by HPLC on a strong anion exchange column and desalted by HPLC on a reverse phase column. Purity and molecular weight of all GalNAc-ASO conjugates were determined by ion-pair LCMS analysis (Supporting Information).

SAR of Tris Based Triantennary GalNAc Conjugated ASOs

We recently showed that Tris-GN3 (Figure 2) conjugation improved the potency of a 5-10-5 MOE gapmer ASO **31** (Table 1) targeting scavenger receptor class B, member 1 (SRB-1) mRNA in mice.[23,24] SRB-1 is ubiquitously expressed in all cell types in the liver and in extrahepatic tissues and ASOs targeting mouse SRB-1was used as a model compound to study the effect of chemical modification on ASO activity in animal models.[39] We used the 5'-Tris-GN3 SRB-1 ASO **32** [24] (Table 1) as a reference GalNAc cluster conjugate for our SAR study. To study the effect of spacer length between the GalNAc sugar and the tris-scaffold on ASGPR binding and activity in cells and in mice, we synthesized 5'-TEA-GN3 ASO **33**, 5'-TBA-GN3 ASO **34**, 5'-THA-GN3 ASO **35** and 5'-TDA-GN3 ASO **36** with spacer lengths of 11.7 Å, 15.0 Å, 18.0 Å and 26.6 Å respectively (Table 1, Figure 2). The spacer length was defined as the distance between the anomeric center of the sugar and the branching point on the cluster.[26]

ASOs **33-36** containing tris scaffold based GalNAc clusters with varying spacer lengths were compared with standard 5'-Tris-GN3 ASO **32** in biological assays (Table 1). First we tested the ability of these GalNAc cluster conjugated ASOs to bind to the ASGR using a competition binding assay.[12,40] ASOs **33-35** containing 5'-TEA, 5'-TBA, THA GN3 exhibited similar binding affinity (Table 1, *K*i 6.1-7.0 nM) to ASGR relative to 5'-Tris-GN3 ASO **32** (Table 1, *K*i 8 nM) while ASO **36** containing 5'-TDA-GN3 with a longer tether (26.6 Å) bound to ASGR with a slightly lower affinity (*K*i 23 nM, Table 1) relative to 5'-Tris-GN3 ASO **32**.[26]

Next we ascertained the potency of ASOs **31-36** in primary mouse hepatocytes which retain ASGR expression in cell culture.[41] The unconjugated and triantennary GalNAc conjugated ASOs **31-36** were delivered without any transfection agents.[42] The triantennary GalNAc modified ASOs **32-35** were more potent than unconjugated ASO **31** (Table 1). Consistent with

ASGR binding data, ASO **36** containing the longer and more hydrophobic spacer was 4 fold less potent than ASO **32**.

We also evaluated the potency of SRB-1 ASOs **32-36** in mice and compared with the unconjugated ASO **31**.[23] Mice (C57BL/6, n=4/group) were injected subcutaneously with a single dose of ASO **32-36** (0.5, 1.5, 5 and 15 mg kg^{-1}). Mice were sacrificed after 72 h, livers were homogenized and analyzed for reduction of SRB-1 mRNA. As expected, all GalNAc cluster conjugated ASOs **32-36** showed improved potency (Table 1) relative to unconjugated ASO **31** (Table 1). ASOs **32-35** exhibited similar potency (ED_{50} 2.4- 4.2 mg kg^{-1}, Table 1) and ASO **36** was less potent (ED_{50} 7.2 mg kg^{-1}). ASOs used in this study were well tolerated with no elevations in plasma transaminases or organ weights (data not shown).

SAR of Triacid Based Triantennary GalNAc Conjugated ASOs

The triacid scaffold (Figure 2) represents a simplified starting point for the synthesis of triantennary GalNAc clusters using the commercially available and inexpensive nitromethanetrispropionic acid starting intermediate.[33] The triacid-scaffold is slightly more hydrophobic as compared to the tris-scaffold as it lacks the oxygen atoms near the branching point on the scaffold (Figure 2). 5'-TAH-GN3 ASO **37**, (spacer length 20.8 Å, Table-1, Figure 2), 5'-TAP-GN3 ASO **38** (spacer length 19.1 Å), 5'-TA-GN3 ASO **39**, (spacer length 15.3 Å), 5'-TAB-GN3 ASO **40**, (spacer length 12.7 Å) and 5'-TAE-GN3 ASO **41** (spacer length 10.1 Å) were synthesized using reported procedures.[33]

In general, ASOs containing 5'-Triacid GN3 with varying spacer lengths exhibited similar binding affinity (*K*i 6.2-10 nM, Table 1) to ASGR relative to 5'-Tris-GN3 ASO **32,** except for 5'-TAB GN3 ASO **40** which showed slightly lower binding (*K*i 26.0 nM, Table 1,

Figure 2). The potency of ASOs **37-41** in mouse primary hepatocytes was determined using the procedure described for the tris-conjugates.[42] The GalNAc cluster modified SRB-1 ASOs **37-41** were more potent (Table 1, Figure 2) than the parent ASO **31** (Figure-1, Table 1). We also evaluated the potency of SRB-1 ASOs **37-41** in mice**.** ASOs **37-41** were injected subcutaneously to mice (C57BL/6, n=4/group) with a single dose of 0.5, 1.5, 5 and 15 mg $kg^{-1}$and mice were sacrificed after 72 h of dosing. The livers were homogenized and analyzed for reduction of SRB-1 mRNA. Animals treated with ASOs **37-41** exhibited similar potency (ED_{50} 2.4-3.8 mg kg^{-1}, Table-1) to 5'-GN3 ASO **32**. There was no elevation in plasma transaminases or organ weights (data not shown) in the animals treated with these ASOs.

Peptide Scaffold Based Triantennary GalNAc Conjugated ASOs

Bifunctional amino acids such as glutamic acid, aspartic acid or lysine have been used as branching elements for the construction of multiantennary GalNAc ligands.[32] Valentijin *et al*. showed that trivalent GalNAc clusters derived from bis-lysine scaffolds show strong binding to the ASGR in competition binding binging assays.[32] To determine if GalNAc clusters based on amino acid scaffolds could be used for targeting ASOs to hepatocytes, we synthesized 5'-Lys-Lys-H-GN3 ASO **42** (Table 1, Figure 2) using the solution phase conjugation strategy described in Scheme 1. Another triantennary GalNAc cluster which binds the ASGR with high affinity was based on 6-aminohexyl GalNAc assembled on a lysine-glycine scaffold (Figure 2, Lys-Gly-HA-GN3).[43] Solution phase conjugation strategy (Scheme 1) using Pfp esters of corresponding GN3 **10** and **11** (Scheme 1) was used for the synthesis of ASOs **42** and **43** (Table 1).[24]

As expected 5'-peptide scaffold based triantennary GalNAc ASO conjugates **42-43** with varying spacer lengths, exhibited similar binding affinity (*K*i 6.3-10.1 nM, Table-1, Figure 2) to ASGR relative to 5'-Tris-GN3 ASO **32** **(**Table 1). Consistent with the binding affinity,

conjugation of peptide scaffold based triantennary GalNAc improved potency of SRB-1 ASOs **42-43** (IC_{50} 6-30 nM, Table 1, Figure 2) relative to unconjugated SRB-1 ASO **31** (IC_{50} 250 nM, Table 1) in mouse primary hepatocytes.[42] The ASOs **42-43** also demonstrated superior potency (ED_{50} 2.1-2.3 mg kg^{-1}, Table 1) in mice relative to unconjugated ASO **31** (ED_{50} 18.3 mg kg^{-1}, Table 1). All ASOs were well tolerated with no elevations in plasma transaminases or organ weights (data not shown).

Trebler Based Triantennary GalNAc Conjugated ASOs

We also developed a strategy for solid phase assembly of GalNAc clusters using well established phosphoramidite chemistry. We hypothesized that the synthesis of triantennary GalNAc ASO conjugates could be simplified by using this approach.[44] In addition, this approach provides an opportunity to examine the effect of introducing a negatively charged phosphodiester group in the tether of the GalNAc cluster on ASGR binding. In brief, this approach involved sequential coupling of a commercially available trebler phosphoramidite to assemble the triantennary scaffold, followed by coupling of the GalNAc phosphoramidite **21** (Figure 3) to provide 5'-PGN3 SRB-1 ASO **44** (Table 1, Figure 2).

The effect of varying spacer length of triantennary GalNAc cluster has been reported.[26] However, the effect of restricting the spacer flexibility of trivalent GalNAc cluster has not been characterized. In order to understand the effect of restricting flexibility of the spacer between the GalNAc sugar and the branching point on ASGR binding and biological activity we designed 5'-Pip-PGN3 ASO **45** (Table 1, Figure 2). Phosphoramidite based GalNAc cluster synthesis[44] on a solid support was used to synthesize ASO **45** using GalNAc piperidine phosphoramidite **22** (Figure 3, Supporting Information).

ASOs **44-45** containing 5'-PGN3 and 5'-Pip-PGN3 respectively exhibited similar binding affinity (*K*i 20-23 nM, Table-1) to ASGR. However, ASOs **44-45** exhibited weaker ASGR binding relative to 5'-Tris-GN3 ASO **32** (*K*i 8 nM, Table-1). Interestingly, ASOs **44-45** showed differences in their ability to inhibit mRNA expression in hepatocytes and in mouse liver (Table 1). Both ASOs were more potent than unconjugated ASO **31** (Table 1). The ASO **45** containing 5'-Pip-PGN3 with a constrained spacer was 3-4 fold less potent in hepatocytes (IC_{50} 150 nM, Table 1) and in animals (ED_{50} 9.8 mg kg^{-1}, Table 1) relative to ASO **44** (Table 1) as well as ASO **32** containing 5'-Tris-GN3. These ASOs were well tolerated with no elevations in plasma transaminases or organ weights (data not shown).

Hydroxyprolinol Based Triantennary GalNAc Conjugated ASOs

We also explored another approach where a serial incorporation of monomer GalNAc provides the required triantennary GalNAc structure as shown in ASOs **46-48** (Table 1, Figure 2) using non-nucleoside hydroxyprolinol GalNAc phosphoramidites **23-24** (Scheme 3) and **25** (Figure 3).[34,45] This approach eliminates the need for a multistep synthesis of triantennary GalNAc or pre-loading the solid support with the bulky triantennary GalNAc for solid-phase oligonucleotide synthesis. Furthermore, this approach allows investigation of linear arrangement of GalNAc sugars as opposed to the branched arrangement with other clusters.

The biological properties of the hydroxyprolinol GN3 containing ASOs **46-48** (Table 1) were studied.[24] The ASOs **46-48** showed differences in their binding to the ASGR.[40,12] Consistent with GalNAc cluster ASOs based on tris scaffold (ASO **36**, Table 1) binding affinity of ASO **47** (*K*i 40 nM, Figure 1) containing longer spacer chain between GalNAc sugar and the originating point was weaker than ASO **46** (*K*i 12 nM, Table 1). ASO **48** with a similar spacer

chain length as the 3'-HP-D-GN3 ASO **47** (Table 1, Figure 3) but with an additional amide linkage binds tighter (*K*i 9.6 nM) to ASGR, suggesting that enhancing hydrophilicity of long aliphatic spacers improves binding of triantennary GalNAc ASOs to ASGR.

The potency of ASOs **46-48** were determined in mouse primary hepatocytes using the protocol described previously. Consistent with other classes of triantennary GalNAc conjugated ASOs, the ASOs **46-48 (**IC_{50} 30-55 nM, Table 1**)** showed improved potency in mouse primary hepatocytes relative to unconjugated ASO **31** (Table 1, IC_{50} 250 nM). Similarly, ASOs **46-48** were more potent (ED_{50} 2.2 to 4.8 mg kg^{-1}, Table 1) in mouse liver relative to unconjugated ASO **31** (ED_{50} 18.3 mg kg^{-1}, Table 1).

Effect of ASO Backbone Chemistry on the Biological Property of 5'-Tris-GN3, 5'-THA-GN3, 5'-TA-GN3 and 5'-Lys-Lys-H-GN3 Conjugated ASOs

Phosphorothioate modified (PS, Figure 1) ASOs binds more avidly to proteins than phosphodiester (PO, Figure 1) ASOs.[46] PS ASOs are highly (90-98%) protein bound in plasma which facilitates ASO delivery to peripheral tissues.[47] However, non-specific protein binding has been implicated in some of the pro-inflammatory effects of PS ASOs.[48] We determined if reducing the PS content of GalNAc-conjugated ASOs, by replacing some of the PS linkages in the MOE wings with PO linkages (termed mixed-backbone MBB ASOs) could be beneficial. MBB ASOs bind less avidly to plasma and cell-surface proteins, and as a consequence, are eliminated more readily in the urine resulting in 2-3 fold reduced activity in animals (data not shown). We proposed that attaching trivalent GalNAc clusters to MBB ASOs could enhance delivery to hepatocytes. Furthermore, the MBB design used was expected to be metabolically stable, as the more labile DNA-gap region and both ends of the ASO were protected using PS

linkages. We selected Tris-GN3, THA-GN3, TA-GN3 and Lys-Lys-H-GN3 (Figure 2) to profile the effect of GalNAc conjugation on the potency of MBB ASOs in primary hepatocytes and in mice.

A 5'-hexylamino-modified MBB SRB-1 ASO (six PO and 13 PS linkages) was conjugated to 5'-Tris-GN3 **49** (Table 2), 5'-THA-GN3 **50** (Table 2), 5'-TA-GN3 **51** (Table 2) and 5'-Lys-Lys-H-GN3 **52** (Table 2) clusters using the solution phase approach (Scheme 1). Purity and mass of ASOs **49-52** were determined by ion-pair LCMS analysis (Supporting Information).

We compared the potency of the MBB ASOs with the corresponding full PS ASOs **32**, **35**, **39** and **42** (Table 2) in mouse primary hepatocytes and in the liver. We found that the MBB ASOs **49-52** show similar or slightly enhanced potency compared to the corresponding full PS ASOs (ASOs **32**, **35**, **39** and **42** Table-2) in mouse primary hepatocytes and in mouse liver. These data suggest that conjugation of trivalent GalNAc clusters to MBB ASOs can be beneficial for reducing ASO PS content without compromising potency. These designs have the potential to mitigate the non-specific protein binding properties and any resulting hybridization-independent toxicities of full PS ASOs for clinical applications.[49]

5'-Tris-GN3, 5'-THA-GN3, 5'-TA-GN3 and 5'-Lys-Lys-H-GN3 Conjugation Improves Potency of MOE gapmer ASO Targeting Mouse A1AT

We next examined the effect of conjugating selected triantennary GalNAc clusters on the potency of a MBB ASO targeting alpha-1 antitrypsin (A1AT) mRNA in mouse liver. ASOs targeting A1AT were recently evaluated for the treatment of alpha-1 antitrypsin deficiency (AATD) which results from accumulation of mutant A1AT protein in liver.[50] A MOE gapmer

ASO **53** (Figure 4) targeting mouse A1AT was used as the unconjugated control ASO for this study.[50] Synthesis of 5'-Tris-GN3, 5'-THA-GN3, 5'-TA-GN3 and 5'-Lys-Lys-H-GN3 conjugated A1AT ASOs **54-57** (Figure 4) were accomplished by a solution phase coupling of corresponding Pfp esters to 5'-hexylamino ASO (Scheme 1). ASOs **54-57** were characterized by ion-pair LCMS analysis (Supporting Information).

Mice (C57BL/6, 4/group) were injected subcutaneously with A1AT ASO **53** (5, 15 and 45 mg kg^{-1}, Figure 4) and corresponding various GalNAc cluster conjugated ASOs **54-57** (0.6, 2, 6 and 18 mg kg^{-1}, Figure 4) once a week for three weeks. Mice were sacrificed 72 h after the last injection and liver and plasma were analyzed for reductions in expression of A1AT mRNA and protein respectively (Figure 4). We observed a 10-fold enhancement in potency for inhibiting A1AT mRNA and protein expression in animals dosed with GN3 ASOs **54-57** (Figure 4, ED_{50} 1.9-3.2 mg kg^{-1}) relative to unconjugated ASO **53** (ED_{50} 25-27 mg kg^{-1}, Figure 4). The level of plasma transaminases or blood urea nitrogen and organ or body-weights of animals treated with these ASOs were normal (data not shown).

5'-Tris-GN3, 5'-THA-GN3, 5'-TA-GN3 and 5'-Lys-Lys-H-GN3 Conjugation Improves Potency of MOE Targeting Mouse Factor XI

Next we determined the effect of conjugating 5'-Tris-GN3, 5'-THA-GN3, 5'-TA-GN3 and 5'-Lys-Lys-H-GN3 on the potency of a 5-10-5 MOE gapmer ASO **58** (Figure 5) targeting mouse coagulation factor XI (FXI). Here we used a 3-week dosing schedule which helps understand the effect of drug accumulation and metabolism on ASO activity. FXI is a member of the intrinsic coagulation pathway and is expressed specifically in hepatocytes and secreted in blood. Inhibiting FXI activity shows benefits in animal models of thrombosis with a minimal risk

of bleeding.[51-53] Trivalent GalNAc conjugated FXI ASOs **59-62** (Figure 5) were synthesized by conjugation of corresponding trivalent GalNAc Pfp esters to 5'-hexylamino conjugated ASO in solution (Scheme 1). Purity and mass of the ASOs **59-62** were determined by ion-pair LCMS analysis (Supporting Information).

Balb-c mice (n=4/group) were injected subcutaneously with 1, 3, 10 and 30 mg kg^{-1} of unconjugated full PS ASO **58** (Figure 5) and 0.08, 0.23, 0.7, 2 and 6 mg kg^{-1} of 5'-trivalent GalNAc conjugated mixed back-bone ASOs **59-62** (Figure 5) once a week for three weeks. FXI mRNA expression was analyzed from the liver tissues of the treated mice. Trivalent GalNAc conjugated ASOs **59-62** (ED_{50} 0.4-0.6 mg kg^{-1}, Figure 5) showed >20 fold enhancement in potency for reducing FXI mRNA levels in liver relative to unconjugated full PS ASO **58** (8.7 mg kg^{-1}, Figure 5). Consistent with other studies all ASOs were well tolerated with no elevations in serum transaminases or organ or body weight changes (data not shown).

SAR to Identify Optimized Linker Chemistry for Attaching Triantennary GalNAc to ASOs

We previously showed that the 3'-Tris-GN3 cluster is detached by metabolism to liberate the parent ASO in the liver.[23] In that study we used a PO-linked deoxyadenosine (dA) nucleotide as a linker moiety between the GalNAc cluster and the ASO to facilitate metabolism. Further studies showed that the first site of metabolism of GalNAc-ASO conjugates was the glycosidic bond to the GalNAc sugars suggesting that the dA linker moiety is not required. To further probe the importance of the PO dA linker moiety on potency, we evaluated ASO conjugates **63**, **64** and **65** (Table 3) where the PO dA was replaced with PO dT, PO MOE A and PO MOE T respectively. In addition, we also evaluated ASO conjugate **66** (Table 3) where the Tris-GN3 cluster was directly attached to the ASO via a 5'-hexylamino PO linkage.

ASOs **63-66** showed similar potency for reducing SRB-1 mRNA in mouse primary hepatocytes. Interestingly, 5'-Tris-GN3 ASO **66** (IC_{50} 9 nM, Table 3) with only the hexylamino PO linker between the GalNAc cluster and the ASO showed improved potency relative to the other ASOs tested in the study. Next we tested the potency of **63-66** (Table 3) for inhibiting SRB-1 mRNA expression in mouse liver. Mice (C57BL/6, n=4/group) were injected subcutaneously with a single dose of ASOs **63-66** (0.5, 1.5, 5 and 15 mg kg^{-1}). After 72 h of dosing mice were sacrificed and analyzed for reduction of SRB-1 mRNA expression in liver. All the tris-GN3 ASO conjugates exhibited similar potency (ED_{50} 1.8-2.8 mg kg^{-1}, Table-3) suggesting that the PO dA or other nucleotide linker moieties between the GalNAc cluster and the ASO are not required for optimal potency enhancement in mice and just a hexylamino PO linkage is sufficient.

5'-Tris-GN3, 5'-THA-GN3, 5'-TA-GN3, 5'-Lys-Lys-H-GN3 and 3'-HP-H-GN3 Conjugation Improves Potency of ASO Targeting Human TTR in Transgenic Mice.

We next studied the effect of conjugating triantennary GalNAc clusters on the potency of a MOE gapmer ASO **67** (Figure 6) targeting human Transthyretin (TTR) in transgenic mouse models. The unconjugated ASO **67** is currently being evaluated in humans for the treatment of TTR-associated polyneuropathy and has shown ~75% reduction in TTR protein in a phase 1 trial at a dose of 300 mg/week (~4 mg/kg/week).[54] Triantennary GalNAc conjugated ASOs **68-72** (Figure 6) were synthesized using similar procedure described in the previous sections. ASOs **68-72** were characterized by ion-pair LCMS analysis (Supporting Information). In ASO **68-72** we used only the hexylamino PO linker for attaching the triantennary GalNAc at the 5'-end of the ASOs.

Human transgenic mice (TTR-Ile84Ser, n=4/group) were injected subcutaneously with the full PS ASO **67** (6, 20 and 60 mg kg^{-1}, Figure 6) and 5'-trivalent GalNAc conjugated mixed backbone ASOs **68-72** (0.6, 2 and 6 mg kg^{-1}) once a week for three weeks. Mice were sacrificed 72 h after last injection and analyzed for reduction of hTTR mRNA in liver and for reduction of hTTR protein in mouse plasma relative to saline treated control mice. All trivalent GalNAc conjugated mixed back-bone ASOs **68-72** (ED_{50} 0.6-0.8 mg kg^{-1}, Figure 6) showed >20 fold enhancement in potency for reducing hTTR mRNA in liver and hTTR protein (ED_{50} 1.3-1.6 mg kg^{-1}) in mouse plasma relative to unconjugated full PS ASO **67** (Figure 6). ASOs **67-72** were well tolerated with no elevations in serum transaminase levels or organ weight changes (Supporting Figure S1-S7).

To ascertain if the improved potency was a result of enhanced delivery to liver, tissue concentration of TTR ASOs **67-72** in the livers of treated mice were quantitated.[23,55,56] We observed increased liver exposure of trivalent GalNAc conjugated ASOs **68-72** (95.6 to 125.9 µg g^{-1} tissue, Table 4) relative to unconjugated ASO **67** (61.6 µg g^{-1} tissue, Table 4). The 5'-GalNAc ASO conjugates **68-71** with PO linkers were fully metabolized to release the parent ASO **67**. These data further established that a hexylamino PO linker between the GalNAc cluster and the ASO is sufficient to liberate the parent ASO by metabolism for 5'-GalNAc ASO conjugates. In contrast, the 3'-HP-H-GN3 ASO **72** was not completely metabolized to the parent ASO **67**. Analysis of livers from mice treated with ASO **72** showed that 20-30% of the extracted oligonucleotide had remnants of various linker moieties still attached to the ASO, thus making these designs less interesting.

Toxicological Evaluation of 5'-Tris-GN3, 5'-THA-GN3, 5'-TA-GN3, 5'-Lys-Lys-H-GN3 and 3'-HP-H-GN3 Conjugated ASO Targeting Mouse ApoC III

Next we evaluated nonclinical safety of 5'-Tris-GN3, 5'-THA-GN3, 5'-TA-GN3, 5'-Lys-Lys-H-GN3 and 3'-HP-H-GN3 conjugated ASOs in mice. First we synthesized 5'-Tris-GN3, 5'-THA-GN3, 5'-TA-GN3, 5'-Lys-Lys-H-GN3 and 3'-HP-H-GN3 conjugated ASOs **74-78** (Figure 7) of unconjugated ASO **73** (Figure 7) targeting mouse apolipoprotein C-III (apoC-III) mRNA.

We studied the potency of ASOs **74-78** to inhibit apoC-III mRNA in mice and compared with unconjugated apoC-III ASO **73** (Figure 7). Mice (C57BL/6, n=4/group) were injected subcutaneously with a single dose of ASO **73** (2, 6, 20 and 60 mg kg^{-1}) and ASOs **74-78 (**0.6, 2, 6 and 20 mg kg^{-1}). Mice were sacrificed after 72 h, livers were homogenized and analyzed for reduction of apoC-III mRNA. As expected, ASOs **74-78** containing structurally different GalNAc clusters (ED_{50} 6.1-7.3 mg kg-1, Figure 7) were 7-8 fold more potent than unconjugated ASO **73** (ED_{50} 50.0 mg kg-1, Figure 7).

Subsequent, we assessed the non-clinical safety of unconjugated ASO **73** and trivalent GalNAc conjugated ASOs **74-78** (Figure 7) in mice. Mice (Male CD-1, n = 8/group) were injected subcutaneously with a dose of unconjugated ASO **73** 100 mg kg^{-1} and equal mole of ASO **74-78** **(**130 mg kg^{-1}) week 0 loading dose day 1, 3 and 5 then once a week for 6 weeks. At termination of the study, the various endpoints were assessed 48 h after the last dose. The ASOs were administered at doses far in excess to relevant therapeutic doses. ASO **73** decreased liver apoC-III mRNA level down to 16% of PBS, whereas the trivalent GalNAc conjugated ASOs decreased liver apoC-III mRNA level down to 4 to 6% of PBS level (p-Value <0.01). While trivalent GalNAc conjugated apoC-III ASOs were more potent than unconjugated ASO **73**, all the GalNAc cluster conjugated ASOs **74-78** were as well tolerated as ASO **73** causing minimal changes, none of them were considered adverse (Figure 8). The weight of the liver, kidneys, spleen and heart relative to the body weight of animals treated with ASOs **74-78** were not

significantly changed compared to ASO **73** (Figure 8). None of the GalNAc conjugated ASOs caused any significant change in liver function measured at 6 weeks, 48 h post dose alanine transaminase (ALT) and aspartate aminotransferase (AST) (Figure 8). There was no significant evidence of inflammation caused by ASOs **74-78** compared to ASO **73** as measured by changes in white blood cell count (WBC) or the chemokine MIP-1β plasma level (Figure 8). Histopathological assessment (data not shown) of the liver and kidneys further demonstrated that the trivalent GalNAc conjugated ASOs were all well tolerated at this dose level and clearly shows an improvement in therapeutic index over unconjugated ASO **73**.

CONCLUSIONS

In conclusion, we report the detailed structure-activity relationships for enhancing ASO potency via ASGR-mediated delivery of triantennary GalNAc-ASO conjugates to hepatocytes. GalNAc clusters assembled from six distinct branched or amino acid scaffolds (abbreviated Tris, Triacid, Lys-Lys, Lys-Gly, Trebler and Hydroxprolinol) were synthesized and attached to ASOs using simplified solution-phase or phosphoramidite based methods. Within each cluster, the length and hydrophobicity of the tether attaching the GalNAc sugar to the branching point on the scaffold was varied to determine the optimal tether length and linker chemistry.

The GalNAc ASO conjugates were evaluated for ASGR binding and for activity in cell culture and in mice where tethers as short as 6 atoms (10.1 Å) were tolerated but longer hydrophobic tethers reduced ASGR affinity and biological activity by 2-4 folds. These results were somewhat surprising and contrary to previously established rules for ASGR binding which suggested that tether lengths of ~20 Å are optimal. We also found that the amide linkages in the tethers of GalNAc conjugates can be replaced with negatively charged phosphodiester linkages

without adversely affecting ASGR binding or activity of the conjugates. While conceptually attractive, these designs generally reduced synthesis yields because of incomplete couplings (5'-Trebler) or metabolism (3'-hydroxyprolinol) and were less preferred.

We also evaluated if GalNAc conjugation could enhance the activity of mixed-backbone (MBB) ASOs in mice where some of the PS linkages from the wing region were replaced with PO. MBB ASOs are generally less active in animals as reducing PS content lowers ASO avidity for plasma and cell-surface proteins which is important for promoting ASO uptake into cells and tissues. MBB ASO designs have the potential to mitigate hybridization-independent toxicities resulting from non-specific interactions of ASOs with certain cellular proteins.[49] We found that GalNAc conjugates of MBB ASOs show similar or enhanced activity compared to full PS designs and thus provide chemical design alternatives for enhancing tolerability while improving activity. Further refining of the linker moiety between the GalNAc cluster and the ASO showed that GalNAc clusters linked to ASOs via a simple hexylamino phosphodiester linkage were optimal.

After the initial profiling studies, five structurally distinct GalNAc clusters were chosen for more extensive evaluation using multiple ASO sequences targeting mouse alpha-1-antitrypsin (A1AT), mouse coagulation Factor XI, mouse apoC-III and human TTR in wild-type or transgenic mice. Most GalNAc ASO conjugates exhibited excellent potencies (ED_{50} 0.5–2 mg/kg) for reducing the targeted mRNA and protein using single and multiple dosing schedules. Selected GalNAc ASO conjugates were also well tolerated at high doses (130 mg/kg/week/6 weeks) in mouse models used for assessing the potency and toxicity of ASO drug candidates. This work culminated in the identification of a simplified tris-based GalNAc cluster (THA-GN3, Figure 9), which can be efficiently assembled using readily available starting materials and

conjugated to ASOs using a solution phase strategy. A THA-GN3 conjugate of an ASO targeting apolipoprotein(a) was recently shown to be 30-fold more potent in humans relative to the parent ASO.[57] GalNAc-ASO conjugates thus represent a viable strategy for enhancing ASO potency in the clinic without adding significant complexity or cost to existing protocols for oligonucleotide synthesis and manufacturing.

EXPERIMENTAL SECTION

Synthesis of Conjugation of 5'-trivalent GalNAc conjugated ASOs in solution. To a solution of 5'-hexylamino ASO in 0.1 M sodium tetraborate buffer, pH 8.5 (2 mM) a solution of GalNAc PFP ester **1-11** (3 mole equivalent, Scheme 1) dissolved in DMSO (40 mM) was added and the reaction mixture was stirred at room temperature for 3h. Concentrated aqueous ammonia was added (5 x reaction volume) and stirred at room temperature for 4 h. Reaction mixture concentrated under reduced pressure and residue dissolved in water and purified by HPLC on a strong anion exchange column (GE Healthcare Bioscience, Source 30Q, 30 µm, 2.54 x 8 cm, A = 100 mM ammonium acetate in 30% aqueous CH_3CN, B = 1.5 M NaBr in A, 0-60% of B in 60 min, flow 14 mL min^{-1}). The residue was desalted by HPLC on reverse phase column to yield the 5'-trivalent GalNAc conjugated ASOs in an isolated yield of 62-80%. The ASOs were characterized by ion-pair-HPLC-MS analysis with Agilent 1100 MSD system.

Synthesis of 3'-HP-H-GN3 ASOs (46, 72, 78) 3'-HP-D-GN3 ASO (47) and 3'-HP-HAH-GN3 ASO (48): Antisense oligonucleotides were synthesized at 40 µmol scale using UnyLinker™ solid support functionalized by modified nucleoside or GalNAc cluster. For the synthesis of 3'-HP-H-GN3 ASOs **46**, **72**, **78** 0.1 M solution of GalNAc phosphoramidite **23** (Scheme 3) and for the synthesis of ASO **47** GalNAc phosphoramidite **24** (Scheme 3) and for ASO **49** phosphoramidite **25** (Figure 4) in 40% dichloromethane in acetonitrile was used. First

phosporamidites **23-25** sequentially coupled three times on a UnyLinker™ solid support and subsequently required nucleoside phosphoramidites were coupled to synthesize the 3'-trivalant GalNAc conjugated ASOs. A solution of all other phosphoramidites in acetonitrile (0.1 M), and standard oxidizing and capping reagents were used. An extended coupling time of 5 minutes was used for incorporation of the 2'-*O*-MOE modified nucleotides. For each of the modified analogs 4-fold excess of 2'-*O*-MOE modified nucleoside 3'-phosphoramidite and GalNAc phosphoramidites **23-25** were delivered with a 12 minute coupling time. The 5′-end dimethoxytrityl group was left on to facilitate purification. Post-synthetically, all oligonucleotides were treated with 1:1 triethylamine: acetonitrile to remove cyanoethyl protecting groups from the phosphorothioate linkages. Subsequently, solid support bearing ASOs were treated with aqueous NH_4OH (28-30 wt%) at 55 ºC for 4 h and then cooled and added 10% (V/V) of 40% methylamine in water. Heating at 55 ^{o}C was continued for additional 12-14 h to cleave trivalent GalNAc conjugated ASOs from support, remove protecting groups, and hydrolyze the UnyLinker™ moiety. Oligonucleotides were purified by ion-exchange chromatography using a gradient of NaBr across a column packed with Source 30Q resin as described before. Pure fractions were desalted using HPLC on a reverse phase column. Purity and mass of oligonucleotides were determined using ion-pair LCMS analysis (Supporting Information).

ASGR Binding Assay. Binding affinity was measured using a competition binding assay using the procedure reported.[23] In brief α1-acid glycoprotein (AGP) (4 mg, 100 nmol) was desialylated by treatment with 50 mM sodium acetate buffer (pH 5) and neuraminidase-agarose (1 U) for 16 h at 37 ^{o}C. Then the protein was iodinated by using published procedure.[58] AGP (1 mg of 1 mg/mL AGP) was mixed with 1 M glycine in 0.25 M NaOH (0.2 mL, pH 10) and added

to a solution containing 10 mM ICl (7 μL), $Na^{125}I$ (2.5 μL) and 1 M glycine in 0.25 M NaOH (25 μL). Mixture was incubated for 10 min at room temperature and free ^{125}I was removed by concentrating sample twice using a 3 kDa molecular weight cut-off spin column. Protein labeling and purity was determined using a HPLC system equipped with an Agilent SEC-3 column (7.8 x 300 mm) and a β-RAM counter. Freshly isolated mouse hepatocytes (10^6 cells/mL) were plated in on 6-well plates in 2 mL of William's medium containing 10 % fetal bovine serum (FBS), 1X non-essential amino acids and 1X sodium pyruvate. Cells were incubated for 16–20 h at 37 ^oC with 5 % CO_2 and washed with medium without FBS prior to binding experiment. Cells were incubated for 30 min at 37 ^oC with 1 mL of competition medium containing 2 % FBS, 10 nM ^{125}I-labeled AGP and GalNAc conjugated ASOs at concentrations ranging from 10^{-11} to 10^{-5} M. Non-specific binding was determined in the presence of 10 mM GalNAc free acid. Cells were washed twice with media without FBS to remove unbound ^{125}I–labeled competitor GalNAc ASO and then lysed using Qiagon's RLT buffer containing 1 % mercaptoethanol. Lysates were briefly freezed (10 min) and then thawed and transferred to round bottom assay tubes and radioactivity measured by a γ counter. Non-specific binding was subtracted before dividing ^{125}I γ counts by the value of the lowest GalNAc conjugated ASO concentration counts. The inhibition curves were fitted according to a single site competition binding equation using a non-linear regression algorithm.

Cell Culture Study. Freshly isolated mouse hepatocytes were placed in wells with growth medium containing 10 % FBS, anti-anti, HEPES, glutamine and varying amounts of ASO or PBS control. Cells were maintained at 37 ^oC and 5 % CO_2 for 16 h and then washed with PBS and lysed. RNA was extracted using Qiagen RNease kit and RNA levels determined by Taqman q-rtPCR using the primers: 5'-TGACAACGACACCGTGTCCT-3' (forward primer), 5'-

ATGCGACTTGTCAGGCTGG-3' (reverse primer) and 5'-CGTGGAGAACCGCAGCCTCCATT-3' (probe). RNA was normalized to total RNA using Ribogreen and all data were performed in triplicate.

Animal Treatment. Animal experiments were conducted in accordance with the American Association for the Accreditation of Laboratory Animal Care guidelines and were approved by the Animal Welfare Committee (Cold Spring Harbor Laboratory's Institutional Animal Care and Use Committee guidelines). The animals were housed in micro-isolator cages on a constant 12-hour light-dark cycle with controlled temperature and humidity and were given access to food and water ad libitum. Blood was collected by cardiac puncture exsanguination with K_2-EDTA (Becton Dickinson Franklin Lakes, NJ) and plasma separated by centrifugation at 10,000 rcf for 4 min at 4°C. Plasma transaminases were measured using a Beckman Coulter AU480 analyzer. Tissues were collected, weighed, flash frozen on liquid nitrogen and stored at -60°C. Reduction of target mRNA expression was determined by real time RT-PCR using 7700 RT-PCR sequence detector (Applied Biosystems). Briefly, RNA was extracted from about 50-100 mg tissue from each mouse using PureLink Pro 96 Total RNA Purification Kit (LifeTechnologies, Carlsbad, CA) and mRNA was measured by qRT-PCR using Express One-Step SuperMix qRT-PCR Kit (Life Technologies, Carlsbad, CA). Primers and probes for the PCR reactions were obtained from Integrated DNA technologies (IDT). The assay is based on a target-specific probe labeled with a fluorescent reporter and quencher dyes at opposite ends. The probe is hydrolyzed through the 5′-exonuclease activity of Taq DNA polymerase, leading to an increasing fluorescence emission of the reporter dye that can be detected during the reaction. RNA transcripts were normalized to total RNA levels using RiboGreen, RNA Quantitation Reagent (Molecular Probes). RiboGreen is an ultrasensitive fluorescent nucleic acid stain which when bound to RNA

has a maximum excitation/emission at ~500nm/525nm. Data are mean values +/- standard deviations.

SRB-1 Mouse Protocol. 6-8 week old C57BL/6 mice (Charles River Laboratories) were treated according to the indicated treatment schedules. The sequences primers and probe used for mouse SRB1 are 5'-TGACAACGACACCGTGTCCT-3' for the forward primer, 5'-ATGCGACTTGTCAGGCTGG-3' for the reverse primer, and 5'-CGTGGAGAACCGCAGCCTCCATT-3' for the probe.

FXI Mouse Protocol. Male Balb-c mice (8 week old, Charles River Laboratories) were treated according to the indicated treatment schedules. The sequences of primers and probe used for mouse FXI were: 5'-ACATGACAGGCGCGATCTCT-3' (forward), 5'-TCTAGGTTCACGTACACATCTTTGC-3' (reverse), and 5'-TTCCTTCAAGCAATGCCCTCAGCAATX-3' (probe). Sandwich enzyme immunoassay was used for measuring mouse FXI plasma protein levels. . Briefly, assay plates were coated with anti-FXI antibody (R&D systems), blocked with 2% BSA and incubated with diluted mouse PPP. After extensive washes FXI protein was detected by incubation with biotinylated anti-FXI antibody (R&D systems), followed by incubation with streptavidin-peroxidase conjugate and TMB substrate (Sigma). FXI plasma protein levels were calculated using serial dilutions of recombinant mouse FXI protein (R&D systems) or serial dilutions of normal mouse plasma.

A1AT Mouse Protocol. C57BL/6 mice (Charles River Laboratories) were treated according to the indicated treatment schedules. The sequences of primers and probe used for mouse A1AT were Forward: 5'-TTCTGGCAGGCCTGTGTTG-3'. Reverse primer: 5'-ATCCTTCTGGGAGGTGTCTGTCT-3'. Fluorescence probe: 5'-

CCCCAGCTTTCTGGCTGAGGATGTTC-3'**.** Plasma A1AT levels protein was measured with an ELISA method according to manufacturer's recommendations (Alpco 41-A1AMS-E01).

TTR Transgenic Mice Protocol. TTR-Ile84Ser transgenic mice were generated and described previously.[59] ASOs or vehicle PBS were injected subcutaneously with indicated dose for indicated periods. Animals were sacrificed 72 h after last dosing. Liver mRNA levels were analyzed as described above and plasma TTR levels and chemistry values were measured on the AU480 Clinical Chemistry Analyzer (Beckman Coulter, CA, USA). Human TTR primers: Forward 5'-CCCTGCTGAGCCCCTACTC-3'. Reverse: 5'-TCCCTCATTCCTTGGGATTG-3'. Fluorescence probe: 5'-ATTCCACCACGGCTGTCGTCA-3'.

ApoC-III Mouse Protocol. ApoC-III ASOs **73-78** subcutaneously administrated to 8-week old male C57BL/6 mice (Jackson Laboratories) at various doses. Mice were sacrificed 72 h after ASO administration and liver collected and flash frozen. RNA was extracted using Invitrogen PureLink Pro 96 Total RNA purification kit and quantified by qPCR using Invitrogen Express One-Step qRT-PCR kit using apoC-III primers: 5'-TGCAGGGCTACATGGAACAA -3' and 5'-CGGACTCCTGCACGCTACTT -3'. Probe with 5' fluorescein and 3' TAMRA: 5'-CTCCAAGACGGTCCAGGATGCGC -3'.

ED_{50} Determination. ED_{50} values were determined with GraphPad Prism 5 software. The log dose of ASOs were plotted against mRNA level relative to untreated controls. The curves thus obtained was fitted using a 4-parameter fit with variable slope and constraining bottom = 0 and top =1.

Cytokine and Chemokine Assay. Plasma was collected from mice by cardiac puncture. MIP-1b levels in the plasma were analyzed using a custom, multiplex immunosorbent assay according

to the manufacturer's protocol (Meso Scale Discovery, Gaithersburg, MD). Multiplex plates pre-coated with capture antibodies for specific analytes were pre-soaked/blocked with calibrator/sample diluent for 30 minutes prior to use. Diluted standards (4 replicates) and samples in duplicate were added to the wells and incubated for two hours. All incubations were performed at room temperature with vigorous shaking (300-1000 rpm). Plates were washed three times with PBS + 0.05% Tween-20 before adding a cocktail of Sulfo-Tag® detection antibodies to each well. After incubating with detection antibodies for two hours, plates were washed three times. Read buffer was added to the wells and the plates immediately imaged using the MSD Sector 2400 imaging system. Data was analyzed using MSD Discovery Workbench® software. Concentrations of all unknown samples were back-calculated using results interpolated from the corresponding standard curve regression using a weighted, four-parameter fit. Final sample concentrations (pg/ml) were calculated by factoring the dilution factor used for each sample.

***N*-(5-Oxo-5-(perfluorophenoxy)pentanoyl)amino-tris-{1-[6-amidohexyl)-2-acetamido-3,4,6-tri-*O*-acetyl-2-deoxy-*β*-D-galacosamine)carboxyethoxymethyl)}-methane (3)**. To a solution of compound **19** (26.7 g, 15.5 mmol) in anhydrous DMF (150 mL) triethylamine (6.4 mL, 46.2 mmol), Pfp-TFA (5.3 mL, 30.8 mmol) were added (color changed from yellow to burgundy). After an h, the reaction was quenched with saturated aqueous sodium bicarbonate solution (150 mL) and resulting solution was extracted with EtOAc (800 mL). The EtOAc layer was washed with 1 N aqueous $NaHSO_4$ solution (400 mL), dried (Na_2SO_4), filtered and concentrated under reduced pressure to yield **3** (29.62 g, quantitative) as light brown foam. ^{1}H NMR (300 MHz, DMSO-d_6): δ 1.18-1.42 (m, 12 H), 1.43-1.66 (m, 12 H,) 1.89-1.98 (m, 9 H), 2.00 (s, 9 H), 2.05 (s, 9 H), 2.09 (br s, 2 H), 2.15 (s, 9 H), 2.28-2.39 (m, 4 H), 2.43 (br t, J = 5.3

Hz, 8 H), 2.77 (t, *J* = 7.4 Hz, 2 H), 3.13-3.30 (m, 6 H), 3.47 (dt, *J* = 9.6, 6.5 Hz, 3 H), 3.64-3.78 (m, 10 H), 3.81-4.05 (m, 9 H), 4.06-4.23 (m, 6 H), 4.68 (d, *J* = 8.32 Hz, 3 H), 5.22-5.32 (m, 3 H), 5.36 (d, *J* = 3.3 Hz, 3 H), 6.43-6.59 (m, 3 H), 6.68-6.77 (m, 2 H);^{19}F NMR (282 MHz, DMSO-d_6): δ -167.7-162.3 (m), -157.8-157.4 (m), -152.9-152.5 (m); ^{13}C NMR (75 MHz, DMSO-d_6): δ 20.7, 23.3, 25.4, 26.4, 29.1, 29.4, 36.7, 39.3, 51.5, 59.8, 61.5, 66.9, 67.6, 69.6, 70.1, 70.6, 101.1, 170.4, 170.5, 170.8, 171.5; HR MS (ESI) calcd for $C_{84}H_{125}F_5N_7O_{36}$ $[M + H]^+$ *m/z* = 1902.8080, found 1902.8078.

1-[6-(*N*-Benzyloxycarbonyl)aminohexyl)-2-acetamido-3,4,6-tri-*O*-acetyl-2-deoxy-*β*-D-galacosamine) (12). GalNAc oxazoline **13** (24.0 g, 72.3 mmol) and compound **14** (16.4, 65.1 mmol) and pre-dried molecular sieves (25 g, 4 Å) were suspended in anhydrous dichloromethane (150 mL). The mixture was stirred at room temperature for 30 min and TMSOTf (6.5 mL, 36.1 mmol) was introduced. After stirring at room temperature for 12 h the reaction mixture was poured into ice cold sodium bicarbonate solution (300 mL) and resulting solution was extracted with dichloromethane (3 x 300 mL). The organic layer was washed with brine (300 mL), dried over Na_2SO_4, filtered and concentrated under reduced pressure. The residue obtained was purified by silica gel chromatography and eluted with 2-5% methanol in dichloromethane to yield compound **12** (27.4 g, 65.4%) as white foam. ^{1}H NMR (300 MHz, DMSO-d_6): δ 1.35-1.43 (m, 4 H), 1.43- 1.65 (m, 4 H), 1.94 (s, 3 H), 2.00 (s, 3 H), 2.05 (s, 3 H), 2.13 (s, 3H), 3.03-3.29 (m, 2 H), 3.48 (dt, *J* = 9.7, 6.5 Hz, 1 H), 3.78-4.04 (m, 3 H), 4.05-4.22 (m, 2 H), 4.65 (d, *J* = 8.3 Hz, 1 H), 4.92 (br s, 1H), 5.03-5.18 (m, 2 H), 5.27 (dd, J=11.26, 3.20 Hz, 1 H), 5.34 (d, J=2.94 Hz, 1 H), 5.96 (br d, *J*=8.58 Hz, 1 H), 7.28-7.41 (m, 5 H); ^{13}C NMR (75 MHz, DMSO-d_6): δ 20.7, 23.4, 25.2, 26.0, 29.0, 29.8, 40.6, 51.6, 61.5, 66.6, 66.9, 69.4, 70.0, 70.6, 100.8, 127.9,

128.1, 128.5, 136.7, 156.6, 170.3, 170.4, 170.4; HRMS (ESI) calcd for $C_{28}H_{41}N_2O_{11}$ $[M + H]^+$ *m/z* = 581.2700, found 581.2722.

Benzyl (6-hydroxyhexyl)carbamate (14). 6-amino-1-hexanol (25.6 g, 220.0 mmol) and sodium carbonate (40.5 g, 380.0 mmol) were suspended in a mixed solvent of 1,4-dioxane (1000 mL) and water (200 mL). To this mixture, benzyl chloroformate (54.6 mL, 380.0 mmol) was added. After stirring at room temperature for 12 h the reaction was quenched with water (400 mL) and extracted with EtOAc (2 x 300 mL). The EtOAc layer was dried over Na_2SO_4, filtered and concentrated under reduced pressure. The residue was crystallized from 50% acetone in hexane. The white solid obtained was filtered to yield **14** (47.2 g, 86%). ^{1}H NMR (300 MHz, d_6-DMSO): δ 1.15-1.45 (m, 4 H), 1.45-1.64 (m, 4 H), 3.21 (q, *J* = 6.7 Hz, 2 H), 3.64 (br t, *J* = 6.2 Hz, 2 H), 4.67-4.89 (br s, 1 H), 5.10 (s, 2 H), 7.29-7.45 (m, 5 H); ^{13}C NMR (75 MHz, DMSO-d_6): δ 25.3, 26.4, 29.9, 32.6, 40.9, 62.7, 66.6, 128.1, 128.5, 136.7, 156.5; HRMS (ESI) calcd for $C_{14}H_{22}NO_3$ $[M + H]^+$ *m/z* = 252.1590, found 252.1592.

3,3'-((2-(5-(Benzyloxy)-5-oxopentanamido)-2-((2-carboxyethoxy)methyl)propane-1,3-diyl)bis(oxy))dipropionic acid (17). To a solution of benzyl glutarate **16** (6.6 g, 29.7 mmol) in DMF (20 mL), HBTU (11.3 g, 29.7 mmol) and *N*,*N*-diisopropylethylamine (6.9 mL, 39.6 mmol) were added and the solution was stirred at room temperature for 15 min. To this a solution of compound **15** (10 g, 19.8 mmol) in DMF (3 mL) was added. The resulting reaction mixture was stirred at room temperature for 12 h. The reaction mixture was diluted with water (200 mL) and extracted with EtOAc (2 x 200 mL). The organic layer was washed with brine (300 mL), dried over Na_2SO_4, filtered and concentrated under reduced pressure. The residue obtained was purified by silica gel column chromatography and eluted with 0-10% methanol in dichloromethane to yield glutaryl derivative of compound **15** (11.2 g, 15.8 mmol, 80%). It was

dissolved in dichloromethane (10 mL) and trifluoroacetic acid (10 mL) was added and the resulting solution was stirred at room temperature for 12 h. The reaction mixture was concentrated under reduced pressure and the residue obtained was crystallized from EtOAc to yield compound **17** (9 g, 80%) as a white solid. ^{1}H NMR (300 MHz, DMSO-d_6): δ 1.72 (m, 2 H), 2.10 (t, *J* = 7.2 Hz, 2 H), 2.35 (t, *J* = 7.6 Hz, 2 H), 2.41 (t, *J* = 6.3 Hz, 6 H), 3.45-3.68 (m, 12 H), 5.11(s, 2 H), 7.00 (s, 1 H), 7.23-7.47 (m, 5 H), 11.82-12.40 (m, 3 H); ^{13}C NMR (75 MHz, DMSO-d_6): δ 20.7, 32.7, 34.5, 34.8, 59.5, 65.3, 66.7, 68.1, 127.8, 127.9, 128.2, 128.4, 136.3, 171.8, 172.5, 172.6; LRMS (ES, positive) *m/z* calcd for $C_{25}H_{35}NO_{12}$: 541.6, found 542.2 $[M + H]^+$.

Bis(perfluorophenyl)3,3'-((2-(5-(benzyloxy)-5-oxopentanamido)-2-((3-oxo-3-(perfluoro phenoxy)propoxy)methyl)propane-1,3-diyl)bis(oxy))dipropionate(18). Compound **17** (20 g, 36.9 mmol) was dissolved in anhydrous DMF (150 mL). To this *N*,*N*-diisopropylethylamine (51.5 mL, 295.5 mmol), Pfp-TFA (25.4 mL, 147.7 mmol) were added slowly. The color of the reaction changed from colorless to burgundy. The reaction mixture was stirred at room temperature for 12 h. The reaction was quenched with aqueous saturated sodium bicarbonate solution and extracted with EtOAc (600 mL). The EtOAc layer was extracted with 1N $NaHSO_4$solution (300 mL), brine (300 mL), dried over Na_2SO_4, filtered and concentrated under reduced pressure. The residue obtained was purified by silica gel column chromatography and eluted with 10-30% EtOAc in hexane to yield **18** (31.9 g, 82.9%) as an orange oil. ^{1}H NMR (300 MHz, DMSO-d_6): δ 1.93 (dd, *J* = 14.1, 7.0 Hz, 2 H), 2.17 (d, *J* = 7.0 Hz, 2 H), 2.39 (t, *J* = 7.4 Hz, 2 H), 2.88 (t, *J* = 5.9 Hz, 6 H), 3.78 (s, 6 H), 3.80 (d, *J* = 5.9 Hz, 6 H), 5.08 (s, 2 H), 5.83 (s, 1 H), 7.28-7.39 (m, 5 H); ^{19}F NMR (282 MHz, DMSO-d_6): δ -162.4-162.2 (m), -157.9-157.7 (m), -153.0-152.8 (m); ^{13}C NMR (75 MHz, DMSO-d_6): δ 20.9, 33.2, 34.2, 36.0, 59.6, 66.1, 66.2,

69.2, 125.0, 128.1, 128.2, 128.6, 136.0, 136.3, 137.9, 139.6, 141.3, 142.8, 167.6, 172.8, 172.9; HRMS (ESI) calcd for $C_{43}H_{33}F_{15}NO_{12}$ $[M + H]^+$ m/z = 1040.1760, found 1040.1753.

***N*-(5-Carboxypentanoyl)amino-tris-{1-[6-amidohexyl)-2-acetamido-3,4,6-tri-*O*-acetyl-2-deoxy-*β*-D-galacosamine)carboxyethoxymethyl)}-methane (19)**: Compound **18** (41g, 39.4 mmol) and compound **12** (77.9 g, 134.1 mmol) were dissolved in a mixture of EtOAc (270 ml) and acetonitrile (270 mL). To this reaction mixture, $Pd(OH)_2/C$ (16.4 g, 20 wt% loading (dry basis), matrix carbon, wet support) was added. The reaction mixture was vigorously stirred at room temperature under H_2 atmosphere for 10 h. The reaction mixture was filtered through a pad of Celite (100 g), washed thoroughly with acetonitrile (4 x 250 mL) and combined filtrate and washing concentrated under reduced pressure. The residue obtained was purified by silica gel column chromatography and eluted with 5-10% methanol in dichloromethane to yield **19** (51.8 g, 75.6%) as white foam. ^{1}H NMR (300 MHz, DMSO-d_6): δ 1.26-1.42 (m, 12 H), 1.44-1.65 (m, 12 H), 1.96 (s, 9 H), 1.98-2.03 (m, 9 H), 2.05 (s, 9 H), 2.10 (s, 2 H), 2.15 (s, 9 H), 2.26 (br d, J = 5.8 Hz, 2 H), 2.35 (br d, J = 5.5 Hz, 2 H), 2.43 (br s, 6 H), 3.22 (br d, J = 6.0 Hz, 6 H), 3.47 (dt, J = 9.4, 6.54 Hz, 3 H), 3.54-3.79 (m, 13 H), 3.80-4.09 (m, 8 H), 4.09-4.25 (m, 6 H), 4.68 (d, J = 8.3 Hz, 3 H), 5.26 (dd, J = 11.2, 3.26 Hz, 3 H), 5.36 (br d, J = 3.2 Hz, 3 H), 6.61 (br s, 1 H), 6.84 (br d, J = 7.8 Hz, 3 H), 7.06 (br s, 3 H); ^{13}C NMR (75 MHz, DMSO-d_6): δ 20.7, 23.3, 25.5, 26.5, 29.2, 29.4, 36.7, 39.4, 51.4, 59.8, 61.5, 66.9, 67.5, 69.3, 69.6, 70.2, 70.6, 101.1, 170.4, 170.6, 171.1, 171.7; HRMS (ESI) calcd for $C_{78}H_{126}N_7O_{36}$ $[M + H]^+$ m/z = 1736.8240, found 1736.8237.

ASSOCIATED CONTENT

*Supporting Information
Experimental details for synthesis of compounds **1-2**, **4**, **10**, **11**, **22-27**, **29-30**; Analytical data for ASOs **20**, **31-78**, Figures S1-7.

AUTHOR INFORMATIONS

Corresponding Author

***Telephone: 760-603-2590**

Email: tprakash@isisph.com

Notes

All authors are employees of Isis Pharmaceuticals.

ABBREVIATIONS USED

ASO, antisense oligonucleotide; MOE, 2'-*O*-(2-methoxyethyl); PS, phosphorothioate; PO, phosphodiester; Pfp, pentafluorophenyl; GN3, trivalent GalNAc cluster; TMSOTf, trimethylsilyl trifluoromethanesulfonate; Pfp-TFA, pentafluorophenyl trifluoroacetate; ES, electrospray; HBTU, 2-(1H-benzotriazol-1-yl)-1,1,3,3-tetramethyluronium hexafluorophosphate; GalNAc, *N*-acetyl galactosamine; HPLC, high-performance liquid chromatography; LCMS, liquid chromatography coupled mass spectrometry; HRMS, high resolution mass spectrometry; LRMS, low resolution mass spectrometry; *m/z*, mass-to-charge ratio; v/v, volume by volume; SRB-1, scavenger receptor class B, member 1; A1AT, alpha-1 antitrypsin; FXI, coagulation factor XI (plasma thromboplastin antecedent); TTR, transthyretin; apoC III, apolipoprotein C-III; UTC, untreated control; BD, before dosing.

REFERENCES

1. Bennett, C. F.; Swayze, E. E. RNA Targeting Therapeutics: Molecular Mechanisms of Antisense Oligonucleotides as a Therapeutic Platform. *Annu. Rev. Pharmacol. Toxicol.* **2010,** *50*, 259-293.
2. Teplova, M. M., G.; Tereshko, V.; Inamati, G. B.; Cook, P. D.; Manoharan, M. and Egli, M. Crystal Strucuture and Improved Antisense Properties of 2'-O-(2-Methoxyethyl)-RNA. *Nat. Struct. Biol.* **1999,** *6*, 535-539.
3. Monia, B. P.; Lesnik, E. A.; Gonzalez, C.; Lima, W. F.; McGee, D.; Guinosso, C. J.; Kawasaki, A. M.; Cook, P. D.; Freier, S. M. Evaluation of 2'-Modified Oligonucleotides Containing 2'-Deoxy Gaps as Antisense Inhibitors of Gene Expression. *J. Biol. Chem.* **1993,** *268*, 14514-14522.
4. Crooke, S. T.; Geary R. S. Clinical Pharmacological Properties of Mipomersen (Kynamro), a Second Generation Antisense Inhibitor of Apolipoprotein B. *Br. J. Clin. Pharmacol.* **2013,** *76*, 269-276.
5. Geary, R. S.; Norris, D.; Yu, R.; Bennett, C. F. Pharmacokinetics, Biodistribution and Cell Uptake of Antisense Oligonucleotides. *Adv. Drug Delivery Rev.* **2015,** *87*, 46-51.
6. Yamamoto, T.; Nakatani, M.; Narukawa, K.; Obika, S. Antisense Drug Discovery and Development. *Future Med. Chem.* **2011,** *3*, 339-365.
7. Sehgal, A.; Vaishnaw, A.; Fitzgerald, K. Liver as a Target for Oligonucleotide Therapeutics. *J. Hepatol.* **2013,** *59*, 1354-1359.

8. Hudgin, R. L.; Pricer, W. E.; Ashwell, G.; Stockert, R. J.; Morell, A. G. The Isolation and Properties of a Rabbit Liver Binding Protein Specific for Asialoglycoproteins. *J. Biol. Chem.* **1974,** *249*, 5536-5543.
9. Spiess, M. The Asialoglycoprotein Receptor: A Model for Endocytic Transport Receptors. *Biochemistry* **1990,** *29*, 10009-10018.
10. Stockert, R. J. The Asialoglycoprotein Receptor: Relationships Between Structure, Function, and Expression. *Physiol. Rev.* **1995,** *75*, 591-609.
11. Steirer, L. M.; Park, E. I.; Townsend, R. R.; Baenziger, J. U. The Asialoglycoprotein Receptor Regulates Levels of Plasma Glycoproteins Terminating with Sialic Acid A2,6-Galactose. *J. Biol. Chem.* **2009,** *284*, 3777-3783.
12. Baenziger, J. U.; Maynard, Y. Human Hepatic Lectin. Physiochemical Properties and Specificity. *J. Biol. Chem.* **1980,** *255*, 4607-4613.
13. Meier, M.; Bider, M. D.; Malashkevich, V. N.; Spiess, M.; Burkhard, P. Crystal Structure of the Carbohydrate Recognition Domain of the H1 Subunit of the Asialoglycoprotein Receptor. *J. Mol. Biol.* **2000,** *300*, 857-865.
14. Geuze, H. J.; Slot, J. W.; Strous, G. J. A. M.; Lodish, H. F.; Schwartz, A. L. Intracellular Site of Asialoglycoprotein Receptor-Ligand Uncoupling: Double-Label Immunoelectron Microscopy During Receptor-Mediated Endocytosis. *Cell* **1983,** *32*, 277-287.
15. Rensen, P. C. N.; van Leeuwen, S. H.; Sliedregt, L. A. J. M.; van Berkel, T. J. C.; Biessen, E. A. L. Design and Synthesis of Novel N-Acetylgalactosamine-Terminated Glycolipids for Targeting of Lipoproteins to the Hepatic Asialoglycoprotein Receptor. *J. Med. Chem.* **2004,** *47*, 5798-5808.

16. Plank, C.; Zatloukal, K.; Cotten, M.; Mechtler, K.; Wagner, E. Gene Transfer into Hepatocytes Using Asialoglycoprotein Receptor Mediated Endocytosis of DNA Complexed with an Artificial Tetra-Antennary Galactose Ligand. *Bioconjugate Chem.* **1992,** *3*, 533-539.

17. Duff, R. J.; Deamond, S. F.; Roby, C.; Zhou, Y.; Ts'o, P. O. P. Intrabody Tissue-Specific Delivery of Antisense Conjugates in Animals: Ligand-Linker-Antisense Oligomer Conjugates. In *Methods in Enzymology*, Phillips, M. I., Ed. Academic Press, New York: 2000; Vol. 313, pp 297-321.

18. Biessen, E. A.; Vietsch, H.; Rump, E. T.; Fluiter, K.; Kuiper, J.; Bijsterbosch, M. K.; van Berkel, T. J. Targeted Delivery of Oligodeoxynucleotides to Parenchymal Liver Cells In Vivo. *Biochem. J.* **1999,** *340*, 783-792.

19. Nair, J. K.; Willoughby, J. L.; Chan, A.; Charisse, K.; Alam, M. R.; Wang, Q.; Hoekstra, M.; Kandasamy, P.; Kel'in, A. V.; Milstein, S.; Taneja, N.; O'Shea, J.; Shaikh, S.; Zhang, L.; van der Sluis, R. J.; Jung, M. E.; Akinc, A.; Hutabarat, R.; Kuchimanchi, S.; Fitzgerald, K.; Zimmermann, T.; van Berkel, T. J.; Maier, M. A.; Rajeev, K. G.; Manoharan, M. Multivalent N-Acetylgalactosamine-Conjugated siRNA Localizes in Hepatocytes and Elicits Robust RNAi-Mediated Gene Silencing. *J. Am. Chem. Soc.* **2014,** *136*, 16958-16961.

20. Sehgal, A.; Barros, S.; Ivanciu, L.; Cooley, B.; Qin, J.; Racie, T.; Hettinger, J.; Carioto, M.; Jiang, Y.; Brodsky, J.; Prabhala, H.; Zhang, X.; Attarwala, H.; Hutabarat, R.; Foster, D.; Milstein, S.; Charisse, K.; Kuchimanchi, S.; Maier, M. A.; Nechev, L.; Kandasamy, P.; Kel'in, A. V.; Nair, J. K.; Rajeev, K. G.; Manoharan, M.; Meyers, R.; Sorensen, B.; Simon, A. R.; Dargaud, Y.; Negrier, C.; Camire, R. M.; Akinc, A. An Rnai Therapeutic

Targeting Antithrombin to Rebalance the Coagulation System and Promote Hemostasis in Hemophilia. *Nat. Med.* **2015,** *21*, 492-497.

21. Bhat, B.; Neben, S.; Tay, J.; Liu, K.; Chau, N.; Hogan, D.; MacKenna, D.; Gibson, N. Rg-101, a GalNAc-Conjugated Anti-Mir Employing a Unique Mechanism of Action by Targeting Host Factor Microrna-122 (Mir-122), Demonstrates Potent Activity and Reduction of HCV in Preclinical Studies. In *AASLD The Liver Meeting*, Washington, DC, 2013.
22. Manoharan, M. Delivery strategies for RNA interference (RNAi) based therapeutics. From Abstracts of Papers, 246th ACS National Meeting & Exposition, Indianapolis, IN, United States, September 8-12, 2013 (2013), MEDI-185.
23. Prakash, T. P.; Graham, M. J.; Yu, J.; Carty, R.; Low, A.; Chappell, A.; Schmidt, K.; Zhao, C.; Aghajan, M.; Murray, H. F.; Riney, S.; Booten, S. L.; Murray, S. F.; Gaus, H.; Crosby, J.; Lima, W. F.; Guo, S.; Monia, B. P.; Swayze, E. E.; Seth, P. P. Targeted Delivery of Antisense Oligonucleotides to Hepatocytes Using Triantennary N-Acetyl Galactosamine Improves Potency 10-Fold in Mice. *Nucleic Acids Res.* **2014,** *42*, 8796-8807.
24. Østergaard, M. E.; Yu, J.; Kinberger, G. A.; Wan, W. B.; Migawa, M. T.; Vasquez, G.; Schmidt, K.; Gaus, H. J.; Murray, H. M.; Low, A.; Swayze, E. E.; Prakash, T. P.; Seth, P. P. Efficient Synthesis and Biological Evaluation of 5'–GalNAc Conjugated Antisense Oligonucleotides. *Bioconjugate Chem.* **2015,** *26***,** 1451-1455.
25. Rensen, P. C. N.; Sliedregt, L. A. J. M.; Ferns, M.; Kieviet, E.; van Rossenberg, S. M. W.; van Leeuwen, S. H.; van Berkel, T. J. C.; Biessen, E. A. L. Determination of the

Upper Size Limit for Uptake and Processing of Ligands by the Asialoglycoprotein Receptor on Hepatocytesin In Vitro and In Vivo. *J. Biol. Chem.* **2001,** *276*, 37577-37584.

26. Biessen, E. A. L.; Beuting, D. M.; Roelen, H. C. P. F.; van de Marel, G. A.; Van Boom, J. H.; Van Berkel, T. J. C. Synthesis of Cluster Galactosides with High Affinity for the Hepatic Asialoglycoprotein Receptor. *J. Med. Chem.* **1995,** *38*, 1538-1546.
27. Rensen, P. C.; van Leeuwen, S. H.; Sliedregt, L.A.; van Berkel, T.J. and Biessen, E.A. Design and Synthesis of Novel N-Acetylgalactosamine-Terminated Glycolipids for Targeting of Lipoproteins to the Hepatic Asialoglycoprotein Receptor. *J. Med. Chem.* **2004,** *47*, 5798-5808.
28. Lee, Y. C.; Lee, R. T. Interactions of Oligosaccharides and Glycopeptides with Hepatic Carbohydrate Receptors. In *Carbohydrates in Chemistry and Biology*, Ernst, B.; Hart, G. W.; Sinaý, P., Eds. Wiley-VCH Verlag GmbH: Weinheim, Germany, 2008; Vol. 4, pp 549-561.
29. Lee, R.; Lee, Y. Preparation of Cluster Glycosides of N-Acetylgalactosamine That Have Subnanomolar Binding Constants Towards the Mammalian Hepatic Gal/GalNAc-Specific Receptor. *Glycoconjugate J.* **1987,** *4*, 317-328.
30. Lee, R. T.; Lin, P.; Lee, Y. C. New Synthetic Cluster Ligands for Galactose/N-Acetylgalactosamine-Specific Lectin of Mammalian Liver. *Biochemistry* **1984,** *23*, 4255-4261.
31. Lee, Y. C.; Townsend, R. R.; Hardy, M. R.; Lönngren, J.; Arnarp, J.; Haraldsson, M.; Lönn, H. Binding of Synthetic Oligosaccharides to the Hepatic Gal/GalNAc Lectin Dependence on Fine Structural Features. *J. Biol. Chem.* **1983,** *258*, 199-202.

32. Valentijn, A. R. P. M.; van der Marel, G. A.; Sliedregt, L. A. J. M.; van Berkel, T. J. C.; Biessen, E. A. L.; van Boom, J. H. Solid-Phase Synthesis of Lysine-Based Cluster Galactosides with High Affinity for the Asialoglycoprotein Receptor. *Tetrahedron* **1997,** *53*, 759-770.

33. Migawa, M. T.; Prakash, T. P.; Vasquez, G.; Wan, W. B.; Low, A.; Yu, J.; Kinberger, G.; Østergaard, M. E.; Swayze, E. E.; Seth, P. P.; Synthesis and Biological Evaluation of 5'-Triantennary GalNAc Conjugated Antisense Oligonucleotides Based on Nitromethane-Trispropionic Acid. **2015** (In Press).

34. Rajeev, K. G.; Nair, J. K.; Jayaraman, M.; Charisse, K.; Taneja, N.; O'Shea, J.; Willoughby, J. L. S.; Yucius, K.; Nguyen, T.; Shulga-Morskaya, S.; Milstein, S.; Liebow, A.; Querbes, W.; Borodovsky, A.; Fitzgerald, K.; Maier, M. A.; Manoharan, M. Hepatocyte-Specific Delivery of siRNAs Conjugated to Novel Non-Nucleosidic Trivalent N-Acetylgalactosamine Elicits Robust Gene Silencing In Vivo. *ChemBioChem* **2015,** *16*, 903-908.

35. Nakabayashi, S.; Warren, C. D.; Jeanloz, R. W. New Procedure for the Preparation of Oligosaccharide Oxazolines. *Carbohydr. Res.* **1986**, *150*, C7.

36. Cardona, C. M.; Gawley, R. E. An Improved Synthesis of a Trifurcated Newkome-Type Monomer and Orthogonally Protected Two-Generation Dendrons. *J. Org. Chem.* **2002,** *67*, 1411-1413.

37. Green, M.; Berman, J. Preparation of Pentafluorophenyl Esters of Fmoc Protected Amino Acids with Pentafluorophenyl Trifluoroacetate. *Tetrahedron Lett.* **1990,** *31*, 5851-5852.

38. Prakash, T. P.; Kawasaki, A. M.; Wancewicz, E. V.; Shen, L.; Monia, B. P.; Ross, B. S.; Bhat, B.; Manoharan, M. Comparing In Vitro and In Vivo Activity of 2'-*O*-[2-

(Methylamino)-2-Oxoethyl]- and 2'-*O*-Methoxyethyl-Modified Antisense Oligonucleotides. *J. Med. Chem.* **2008,** *51*, 2766–2776.

39. Murray, S.; Ittig, D.; Koller, E.; Berdeja, A.; Chappell, A.; Prakash, T. P.; Norrbom, M.; Swayze, E. E.; Leumann, C. J.; Seth, P. P. TricycloDNA-Modified Oligo-2'-Deoxyribonucleotides Reduce Scavenger Receptor B1 mRNA in Hepatic and Extra-Hepatic Tissues a Comparative Study of Oligonucleotide Length, Design and Chemistry. *Nucleic Acids Res.* **2012,** *40*, 6135-6143.
40. Baenziger, J. U.; Fiete, D. Galactose and N-Acetylgalactosamine-Specific Endocytosis of Glycopeptides by Isolated Rat Hepatocytes. *Cell* **1980,** *22*, 611-620.
41. Severgnini, M.; Sherman, J.; Sehgal, A.; Jayaprakash, N. K.; Aubin, J.; Wang, G.; Zhang, L.; Peng, C. G.; Yucius, K.; Butler, J.; Fitzgerald, K. A Rapid Two-Step Method for Isolation of Functional Primary Mouse Hepatocytes: Cell Characterization and Asialoglycoprotein Receptor Based Assay Development. *Cytotechnology* **2012,** *64*, 187-195.
42. Koller, E.; Vincent, T. M.; Chappell, A.; De, S.; Manoharan, M.; Bennett, C. F. Mechanisms of Single-Stranded Phosphorothioate Modified Antisense Oligonucleotide Accumulation in Hepatocytes. *Nucleic Acids Res.* **2011,** *39*, 4795-4807.
43. Lee, R. T.; Wang, M.-H.; Lin, W.-J.; Lee, Y. C. New and More Efficient Multivalent Glyco-Ligands for Asialoglycoprotein Receptor of Mammalian Hepatocytes. *Bioorg. Med. Chem.* **2011,** *19*, 2494-2500.
44. Prakash, T. P.; Brad Wan, W.; Low, A.; Yu, J.; Chappell, A. E.; Gaus, H.; Kinberger, G. A.; Østergaard, M. E.; Migawa, M. T.; Swayze, E. E.; Seth, P. P. Solid-Phase Synthesis

of 5′-Triantennary N-Acetylgalactosamine Conjugated Antisense Oligonucleotides Using Phosphoramidite Chemistry. *Bioorg. Med. Chem. Lett.* **2015,** *25*, 4127-4130.

45. Yamamoto, T.; Sawamura, M.; Wada, F.; Harada-Shiba, M.; Obika, S. Serial Incorporation of a Monovalent GalNAc Phosphoramidite Unit into Hepatocyte-Targeting Antisense Oligonucleotides. *Bioorg. Med. Chem.* **2015** doi://dx.doi.org/10.1016/ j.bmc. 2015.11.036
46. Brown, D. A.; Kang, S. H.; Gryaznov, S. M.; DeDionisio, L.; Heidenreich, O.; Sullivan, S.; Xu, X.; Nerenberg, M. I. Effect of Phosphorothioate Modification of Oligodeoxynucleotides on Specific Protein Binding. *J. Biol. Chem.* **1994,** *269*, 26801-26805.
47. Geary, R. S.; Watanabe, T. A.; Truong, L.; Freier, S.; Lesnik, E. A.; Sioufi, N. B.; Sasmor, H.; Manoharan, M.; Levin, A. A. Pharmacokinetic Properties of 2'-*O*-(2-Methoxyethyl)-Modified Oligonucleotide Analogs in Rats. *J. Pharmacol. Exp. Ther.* **2001,** *296*, 890-897.
48. Levin, A. A. A Review of the Issues in the Pharmacokinetics and Toxicology of Phosphorothioate Antisense Oligonucleotides. *Biochim. Biophys. Acta* **1999,** *1489*, 69-84.
49. Lindow, M.; Vornlocher, H.-P.; Riley, D.; Kornbrust, D. J.; Burchard, J.; Whiteley, L. O.; Kamens, J.; Thompson, J. D.; Nochur, S.; Younis, H.; Bartz, S.; Parry, J.; Ferrari, N.; Henry, S. P.; Levin, A. A. Assessing Unintended Hybridization-Induced Biological Effects of Oligonucleotides. *Nat. Biotech.* **2012,** *30*, 920-923.
50. Guo, S.; Booten, S. L.; Aghajan, M.; Hung, G.; Zhao, C.; Blomenkamp, K.; Gattis, D.; Watt, A.; Freier, S. M.; Teckman, J. H.; McCaleb, M. L.; Monia, B. P. Antisense

Oligonucleotide Treatment Ameliorates Alpha-1 Antitrypsin-Related Liver Disease in Mice. *J. Clin. Invest.* **2014,** *124*, 251-261.

51. Crosby, J. R.; Marzec, U.; Revenko, A. S.; Zhao, C.; Gao, D.; Matafonov, A.; Gailani, D.; MacLeod, A. R.; Tucker, E. I.; Gruber, A.; Hanson, S. R.; Monia, B. P. Antithrombotic Effect of Antisense Factor XI Oligonucleotide Treatment in Primates. *Arterioscler. Thromb. Vasc. Biol.* **2013,** *33*, 1670-1678.
52. Zhang, H.; Lowenberg, E. C.; Crosby, J. R.; MacLeod, A. R.; Zhao, C.; Gao, D.; Black, C.; Revenko, A. S.; Meijers, J. C.; Stroes, E. S.; Levi, M.; Monia, B. P. Inhibition of the Intrinsic Coagulation Pathway Factor XI by Antisense Oligonucleotides: A Novel Antithrombotic Strategy with Lowered Bleeding Risk. *Blood* **2010,** *116*, 4684-4692.
53. Bueller, H. R.; Bethune, C.; Bhanot, S.; Gailani, D.; Monia, B. P.; Raskob, G. E.; Segers, A.; Verhamme, P.; Weitz, J. I. Factor XI Antisense Oligonucleotide for Prevention of Venous Thrombosis. *N. Engl. J. Med.* **2015,** *372*, 232-240.
54. Ackermann, E. J.; Guo, S.; Booten, S.; Alvarado, L.; Benson, M.; Hughes, S.; Monia, B. P. Clinical Development of an Antisense Therapy for the Treatment of Transthyretin-Associated Polyneuropathy. *Amyloid* **2012,** *19 Suppl 1*, 43-44.
55. Graham, M. J.; Crooke, S. T.; Monteith, D. K.; Cooper, S. R.; Lemonidis, K. M.; Stecker, K. K.; Martin, M. J.; Crooke, R. M. In Vivo Distribution and Metabolism of a Phosphorothioate Oligonucleotide within Rat Liver after Intravenous Administration. *J. Pharmacol. Exp. Ther.* **1998,** *286*, 447-458.
56. Graham, M. J.; Crooke, S. T.; Lemonidis, K. M.; Gaus, H. J.; Templin, M. V.; Crooke, R. M. Hepatic Distribution of a Phosphorothioate Oligodeoxynucleotide within Rodents Following Intravenous Administration. *Biochem. Pharmacol.* **2001,** *62*, 297-306.

57. Witztum, J. Compelling Results from Isis-Apo(a)-Lrx Phase 1/2a Study. *American Heart Association Scientific Sessions* **2015,** November 7-11, Orlando, Florida, U. S. A.

58. Atsma, D. E.; Kempen, H. J.; Nieuwenhuizen, W.; van 't Hooft, F. M.; Pauwels, E. K. Partial Characterization of Low Density Lipoprotein Preparations Isolated from Fresh and Frozen Plasma after Radiolabeling by Seven Different Methods. *J. Lipid Res.* **1991,** *32*, 173-181.

59. Benson, M. D.; Kluve-Beckerman, B.; Zeldenrust, S. R.; Siesky, A. M.; Bodenmiller, D. M.; Showalter, A. D.; Sloop, K. W. Targeted Suppression of an Amyloidogenic Transthyretin with Antisense Oligonucleotides. *Muscle Nerve* **2006,** *33*, 609-618.

Table 1. ASGR binding and potency of SRB-1 ASOs containing Tris (**32-36**), Triacid (**37-41**), Lys.Lys (**42**), Lys-Gly (**43**), Trebler (**44-45**) and hydroxylprolinol (**46-48**) scaffolds

ASO No.	X: Trivalent GalNAc	Atoms in Linker*	ASGPR *K*i nM	IC_{50} nM	ED_{50} mg kg^{-1}
31	None	None	-	250.3 ± 1.8	18.3 ± 1.1
Tris Based GalNAc Clusters					
32	5’-Tris-GN3	16	8.0 ± 1.2	40.2 ± 1.1	2.4 ± 1.1
33	5’-TEA-GN3	7	6.8 ± 1.6	10.4 ± 1.2	4.2 ± 1.3
34	5’-TBA-GN3	9	7.0 ± 1.3	10.3 ± 1.2	3.5 ± 1.4
35	5’-THA-GN3	11	6.1 ± 1.4	20.1 ± 1.1	3.7 ± 1.2
36	5’-TDA-GN3	17	23.0 ± 1.5	149.8 ± 6.1	7.2 ± 1.5
Triacid Based GalNAc Clusters					
37	5'-TAH-GN3	15	10.3 ±1.2	30.1 ± 1.4	2.2 ± 1.1
38	5'-TAP-GN3	14	10.0 ±1.3	70.3 ± 1.1	2.4 ± 1.0
39	5'-TA-GN3	11	6.2 ±1.2	30.0 ± 1.3	2.6 ± 1.2
40	5'-TAB-GN3	9	8.4 ± 1.2	20.4 ± 1.1	3.8 ± 1.3
41	5'-TAE-GN3	7	26.0 ±1.5	20.4 ± 1.1	3.2 ± 1.3
Lys-Lys and Lys-Gly Based GalNAc Clusters					
42	5'-Lys-Lys-H-GN3	11, 12, 15	10.1 ± 1.4	30.3 ± 1.2	2.1 ± 1.2
43	5'-Lys-Gly-HA-GN3	11, 12	6.3 ± 1.2	6.3 ± 1.2	2.3 ± 1.1
Trebler Based GalNAc Clusters					
44	5'-PGN3	15	20.0 ± 1.3	60.3 ± 1.2	3.1 ± 1.3
45	5'-Pip-PGN3	18	23.0 ± 1.2	149.6 ± 8.4	9.8 ± 1.6
Hydroxyprolinol Based GalNAc Clusters					
46	3’-HP-H-GN3	7	12.0 ± 1.6	40.2 ± 1.1	2.9 ± 1.2
47	3’- HP-D-GN3	13	40.0 ± 1.8	55.3 ± 1.2	4.8 ± 1.4
48	3'-HP-HAH-GN3	14	9.6 ± 1.2	30.3 ± 1.2	2.2 ± 1.1

SRB-1 ASO: 5’-X-$_{o}A_{do}G_{es}{}^{m}C_{es}Te_{s}Te_{s}{}^{m}C_{es}A_{ds}G_{ds}T_{ds}{}^{m}C_{ds}A_{ds}\,T_{ds}G_{ds}A_{ds}{}^{m}C_{ds}T_{ds}Te_{s}{}^{m}Ce_{s}{}^{m}C_{es}T_{es}T_{e}$**;** e: 2’-*O*-MOE, d: DNA, ^{m}C: 5-methylcytidine, s: phosphorothioate, o: phosphodiester; *number of atoms in the linker

Table 2. Potency of SRB-1 full PS and mixed backbone (PO/PS) ASOs containing selected GalNAc clusters in hepatocytes and in mice

ASO No.	X: Trivalent GalNAc	ASO Backbone	IC_{50} nM	ED_{50} mg kg^{-1}
31	None	PS	250.3 ±1.8	18.3 ± 1.1
32	5’-Tris-GN3	PS	40.2 ± 1.1	2.4 ± 1.1
35	5’-THA-GN3	PS	19.8 ± 1.1	2.1 ± 1.2
39	5’-TA-GN3	PS	29.7 ± 1.3	2.6 ± 1.2
42	5'-Lys-Lys-H-GN3	PS	30.3 ± 1.2	2.1 ± 1.2
49	5’-Tris-GN3	PO/PS	8.4 ± 1.1	2.0 ± 1.1
50	5’-THA-GN3	PO/PS	7.9 ± 1.3	1.6 ± 1.1
51	5’-TA-GN3	PO/PS	7.8± 1.1	1.5 ± 1.1
52	5'-Lys-Lys-H-GN3	PO/PS	8.3 ± 1.2	1.4 ± 1.1

SRB-1 full PS ASO 5’-X-$_{o}A_{do}G_{es}{}^{m}C_{es}T_{e}T_{s}T_{e}{}_{s}{}^{m}C_{es}A_{ds}G_{ds}T_{ds}{}^{m}C_{ds}A_{ds}T_{ds}G_{ds}A_{ds}{}^{m}C_{ds}T_{ds}T_{e}{}_{s}{}^{m}C_{e}{}_{s}$ $^{m}C_{es}T_{es}T_{e}$-3’; SRB-1 PO/PS ASO 5’-X-$_{o}A_{do}G_{es}{}^{m}C_{eo}T_{eo}T_{eo}{}^{m}C_{eo}A_{ds}G_{ds}T_{ds}{}^{m}C_{ds}A_{ds}T_{ds}G_{ds}A_{ds}{}^{m}C_{ds}$ $T_{ds}T_{eo}{}^{m}C_{eo}{}^{m}C_{es}T_{es}T_{e}$-3’; e: 2’-*O*-MOE, d: DNA, ^{m}C: 5-methylcytidine, s: phosphorothioate, o: phosphodiester.

Table 3. Potency of SRB-1 ASO containing 5'-Tris-GN3 with different linking chemistries in hepatocytes and mice

ASO No.	Sequence (5' to 3')	IC_{50} nM	ED_{50} mg kg^{-1}
31	**GCTTCAGTCATGACTTCCTT**	250.3 ±1.8	18.3 ± 1.1
32	**Tris-GN3$_o$A$_o$GCTTCAGTCATGACTTCCTT**	40.2 ± 1.1	2.4 ± 1.1
63	**Tris-GN3$_o$T$_o$GCTTCAGTCATGACTTCCTT**	15.4 ± 1.1	2.8 ± 1.2
64	**Tris-GN3$_o$A$_o$GCTTCAGTCATGACTTCCTT**	29.5 ± 1.3	2.5 ± 1.1
65	**Tris-GN3$_o$T$_o$GCTTCAGTCATGACTTCCTT**	24.8 ± 1.2	2.4 ± 1.1
66	**Tris-GN3$_o$GCTTCAGTCATGACTTCCTT**	9.2 ± 1.1	1.8 ± 1.0

All cytosine nucleobases were 5-methyl substituted, Orange letters indicate MOE nucleotides; black letters indicate DNA; All internucleosidic linkages were phosphorothioate modified; o indicates phosphodiester linkages

Table 4. Liver concentration of ASOs targeted to human TTR mRNA containing 5'-Tris-GN3 (**68**), 5'-THA-GN3 (**69**), 5'-TA-GN3 (**70**), 5'-Lys-Lys-H-GN3 (**71**) and 3'-HP-H-GN3 (**72**)

ASO No.	Liver Tissue Concentration ($\mu g\ g^{-1}$)		
	0.6 mg kg^{-1}	2 mg kg^{-1}	6 mg kg^{-1}
67*	-	-	61.6 ± 6.8
68	15.3 ± 3.8	57.4 ± 20.3	118.8 ± 16.0
69	12.1 ± 4.6	52.8 ± 5.4	95.6 ± 10.3
70	10.8 ± 6.3	58.8 ± 3.9	111.6 ± 5.7
71	11.0 ± 4.7	80.2 ± 22.8	117.3 ± 7.5
72	10.2 ± 1.3	66.3 ± 3.9	125.9 ± 25.8

*Liver tissue concentration: ASO **67** 168.1 ± 27 $\mu g\ g^{-1}$ (20 mg kg^{-1}); 339.5 ± 32.6 (60 mg kg^{-1})

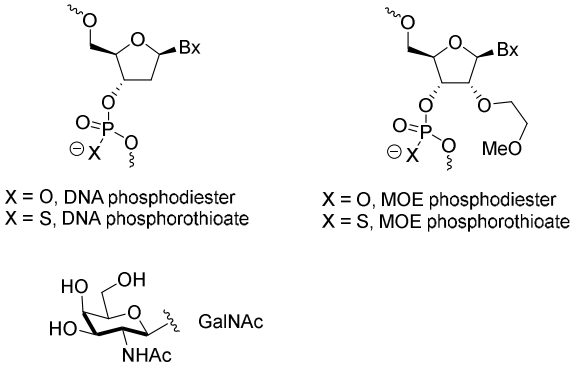

Figure 1. Structures of phosphodiester (PO) and phosphorothioate (PS) DNA and 2'-*O*-methoxyethyl RNA (MOE) nucleotides and *N*-acetylgalactosamine sugar (GalNAc)

Figure 2. Structures of Tris, Triacid, Lys-Lys, Lys-Gly, Trebler and Hydroxyprolinol scaffold based GalNAc cluster conjugated ASOs

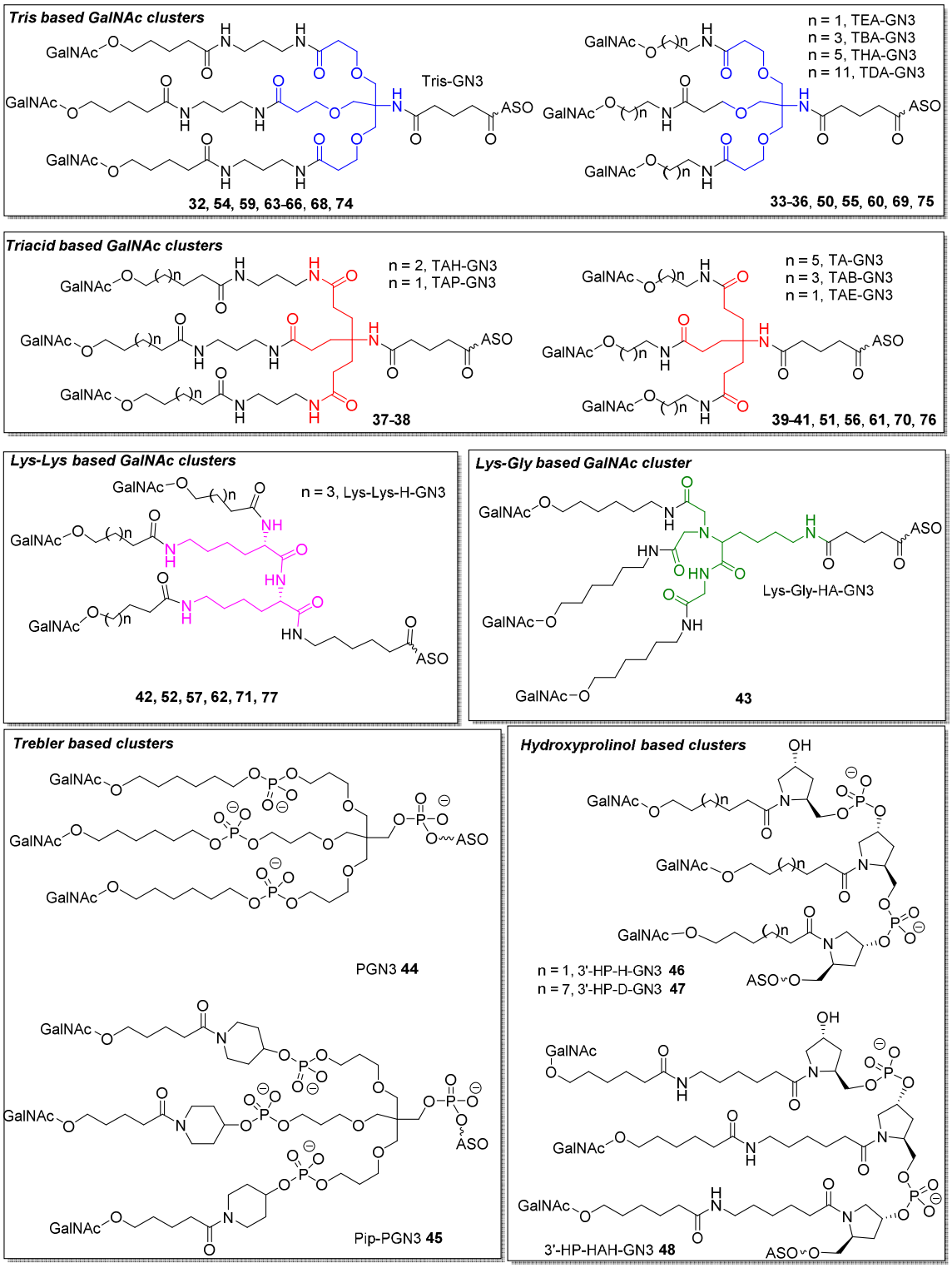

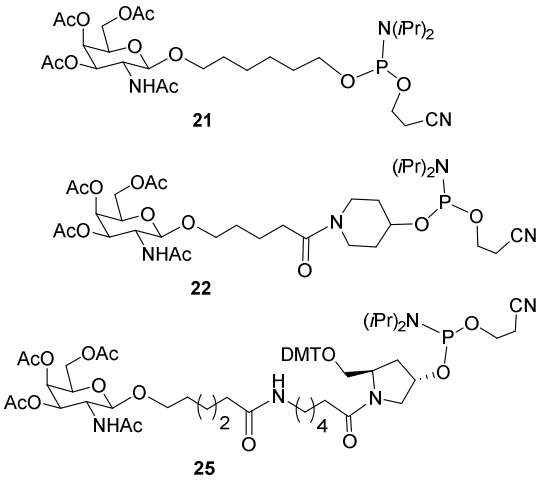

Figure 3: Structures of GalNAc phosphoramidites **21, 22** and **25**

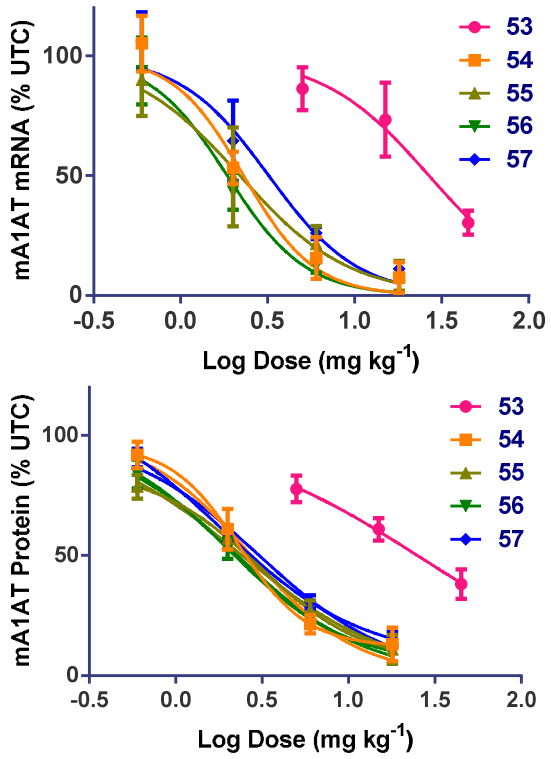

ASO No.	X: Trivalent GalNAc	mRNA ED_{50} mg kg^{-1}	Protein ED_{50} mg kg^{-1}
53	None	27	25
54	5'-Tris-GN3	2.3	2.7
55	5'-THA-GN3	2.2	2.4
56	5'-TA-GN3	1.9	2.3
57	5'-Lys-Lys-H-GN3	3.2	3.0

Figure 4. Potency of 5'- trivalent GalNAc conjugated alpha-1 antitrypsin (mA1AT) ASOs in mice; mice were administered subcutaneously ASO-**53** at 5, 15, 45 mg kg^{-1} and ASOs **54-57** at 0.6, 2, 6 and 18 mg kg^{-1} once a week for 3 weeks; mA1AT ASOs **53-57**: 5'-X-$_{o}A_{do}A_{es}{}^{m}C_{es}{}^{m}C_{es}{}^{m}C_{es}A_{es}A_{ds}T_{ds}T_{ds}{}^{m}C_{ds}A_{ds}G_{ds}A_{ds}A_{ds}G_{ds}G_{ds}A_{es}A_{es}G_{es}G_{es}A_{e}$-3' ASO doses not given**;** e: 2'-*O*-MOE, d: DNA, ^{m}C: 5-methyl cytidine, s: phosphorothioate, o: phosphodiester

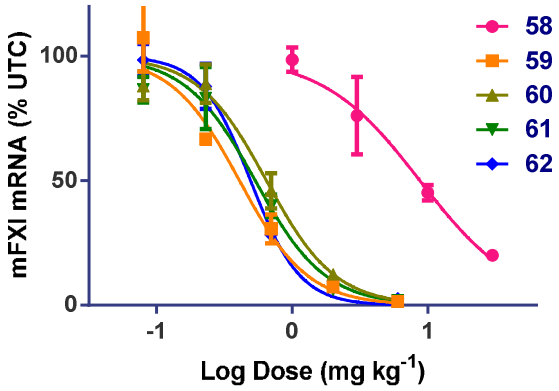

ASO #	X: Trivalent GalNAc	mRNA ED_{50} mg kg^{-1}
58	None	8.7
59	5'-Tris-GN3	0.4
60	5'-THA-GN3	0.6
61	5'-TA-GN3	0.5
62	5'-Lys-Lys-H-GN3	0.5

Figure 5. Potency of 5'-trivalent GalNAc conjugated FXI (mFXI) ASOs in mice; mice were administered subcutaneously ASO-**58** at 1, 3, 10, 30 mg kg^{-1} and ASOs **59**-**62** at 0.08, 0.23, 0.7, 2, 6 mg kg^{-1} once a week for 3 weeks. Full PS mFXI ASO **58**: 5'-$T_{es}G_{es}G_{es}T_{es}A_{es}A_{ds}T_{ds}$ $^{m}C_{ds}{}^{m}C_{ds}A_{ds}$ $^{m}C_{ds}T_{ds}T_{ds}T_{ds}{}^{m}C_{ds}A_{es}G_{es}A_{es}G_{es}G_{e}$-3'**;** Mixed backbone (PO/ PS) mFXI ASO**s 59**-**62**: 5'-X-$_{o}A_{do}T_{es}G_{eo}G_{eo}T_{eo}A_{eo}A_{ds}T_{ds}$ $^{m}C_{ds}{}^{m}C_{ds}A_{ds}{}^{m}C_{ds}T_{ds}$ $T_{ds}T_{ds}{}^{m}C_{ds}A_{eo}G_{eo}A_{es}G_{es}G_{e}$-3'; e: 2'-*O*-MOE, d: DNA, ^{m}C: 5-methyl cytidine, s: phosphorothioate, o: phosphodiester

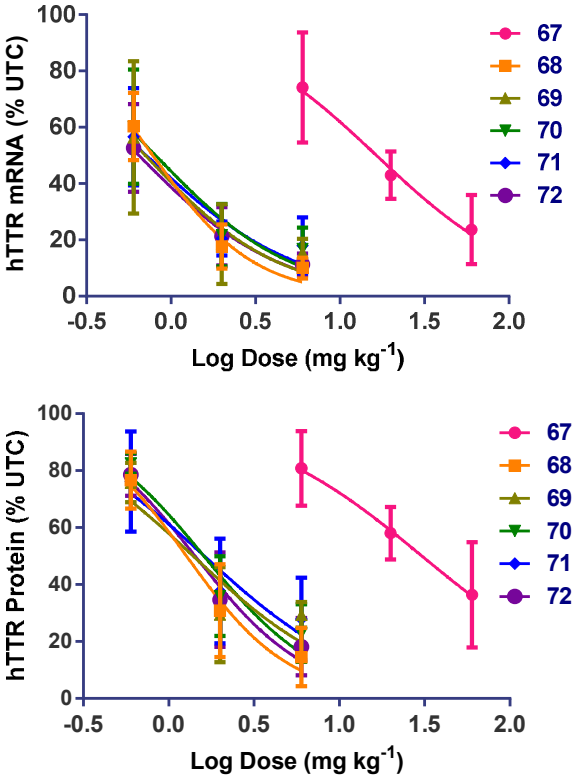

ASO No.	X: Trivalent GalNAc	mRNA ED_{50} mg kg^{-1}	Protein ED_{50} mg kg^{-1}
67	None	16.4	30.5
68	5'-Tris-GN3	0.8	1.3
69	5'-THA-GN3	0.7	1.4
70	5'-TA-GN3	0.8	1.6
71	5'-Lys-Lys-H-GN3	0.7	1.6
72	3'-HP-H-GN3	0.6	1.4

Figure 6. Potency of 5'-trivalent GalNAc conjugated human TTR (hTTR) mixed backbone ASOs in transgenic mice; transgenic mice were administered subcutaneously ASO-**67** at 6, 20, 60 mg kg^{-1} and ASOs **68-72** at 0.6, 2 and 6 mg kg^{-1} once a week for 3 weeks; ASO **67**: 5'-$T_{es}{}^{m}C_{es}T_{es}T_{es}$ $G_{es}G_{ds}T_{ds}T_{ds}$ $A_{ds}{}^{m}C_{ds}A_{ds}T_{ds}G_{ds}A_{ds}$ $A_{ds}A_{es}T_{es}$ $^{m}C_{es}{}^{m}C_{es}{}^{m}C_{e}$-3'; ASOs **68-71**:5'-X-$_{o}T_{es}{}^{m}C_{eo}T_{eo}T_{eo}$ $G_{eo}G_{ds}T_{ds}T_{ds}$ $A_{ds}{}^{m}C_{ds}A_{ds}$ $T_{ds}G_{ds}A_{ds}AdsA_{eo}T_{eo}$ $^{m}C_{es}{}^{m}C_{es}{}^{m}C_{e}$-3; ASO **72**: 5'-$T_{es}{}^{m}C_{eo}T_{eo}T_{eo}G_{eo}G_{ds}$ $T_{ds}T_{ds}A_{ds}{}^{m}C_{ds}$ $A_{ds}T_{ds}$ $G_{ds}A_{ds}A_{ds}$ $A_{eo}T_{eo}{}^{m}C_{es}{}^{m}C_{es}{}^{m}C_{eo}A_{do}$-X-3'; e: 2'-*O*-MOE, d: DNA, ^{m}C: 5-methylcytidine, s: phosphorothioate, o: phosphodiester

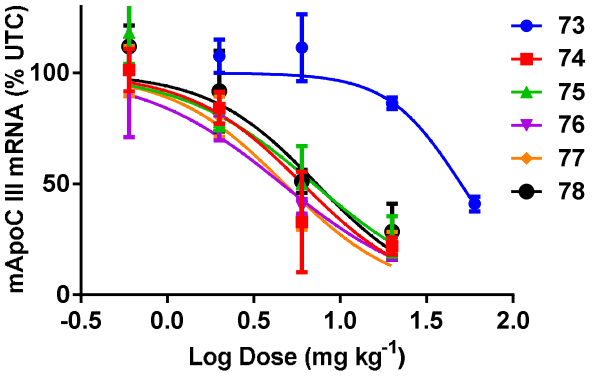

ASO No.	X: Trivalent GalNAc	mRNA ED_{50} mg kg^{-1}
73	None	50.0
74	5'-Tris-GN3	6.1
75	5'-THA-GN3	7.0
76	5'-TA-GN3	4.6
77	5'-Lys-Lys-H-GN3	5.0
78	3'-HP-H-GN3	7.3

Figure 7. Potency of 5'-trivalent GalNAc conjugated ApoC III (apoC III) ASOs in mice; mice were administered subcutaneously ASO **73** at 2, 6, 20, 60 mg kg^{-1} and ASOs **74-78** at 0.6, 2, 6, and 20 mg kg^{-1} once; Full PS ASO **73** sequence: 5'-$^{m}C_{es}A_{es}G_{es}{}^{m}C_{es}T_{es}T_{ds}T_{ds}A_{ds}T_{ds}T_{ds}A_{ds}G_{ds}G_{ds}G_{ds}A_{ds}{}^{m}C_{es}A_{es}G_{es}{}^{m}C_{es}A_{e}$-3'; ASO **74-77** 5'-X-$_{o}{}^{m}C_{es}A_{es}G_{es}{}^{m}C_{es}T_{es}T_{ds}T_{ds}A_{ds}T_{ds}T_{ds}A_{ds}G_{ds}G_{ds}G_{ds}A_{ds}{}^{m}C_{es}A_{es}G_{es}{}^{m}C_{es}A_{e}$-3'; ASO **78** 5'-$^{m}C_{es}A_{es}G_{es}{}^{m}C_{es}T_{es}T_{ds}T_{ds}A_{ds}T_{ds}T_{ds}A_{ds}G_{ds}G_{ds}G_{ds}A_{ds}{}^{m}C_{es}A_{es}G_{es}{}^{m}C_{es}A_{eo}A_{do}$-X-3'e: 2'-*O*-M OE, d: DNA, ^{m}C: 5-methyl cytidine, s: phosphorothioate, o: phosphodiester

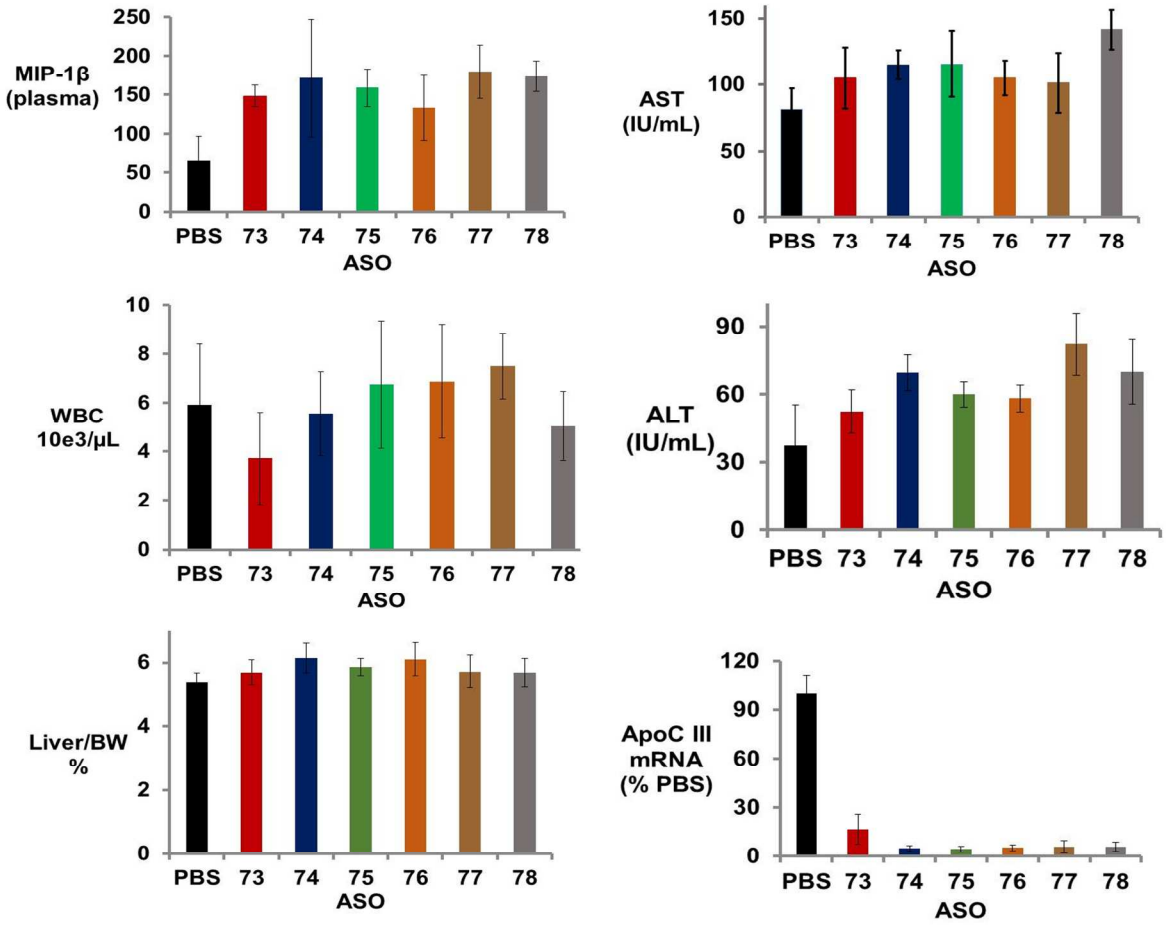

Figure 8. The efficacy and tolerability of apoC-III ASOs **73-78** was assessed in CD-1 mice. The mice were administered subcutaneously on days 1, 3 and 5 then once a week for 6 weeks with 100 mg/kg ASO **73** or 130 mg/kg of ASO **74-78**. The various endpoints were measured 48 h after the last dose. Liver apoC-III mRNA level was measured by RT-PCR to determine the efficacy. Effect of the ASOs on liver function were assessed by measuring increase in liver/body weight (BW) % as well as by measuring ALT and AST levels. Effects of the ASOs on inflammation were assessed by measuring increase in white blood cells count (WBC) as well as by measuring plasma chemokine MIP-1β levels.

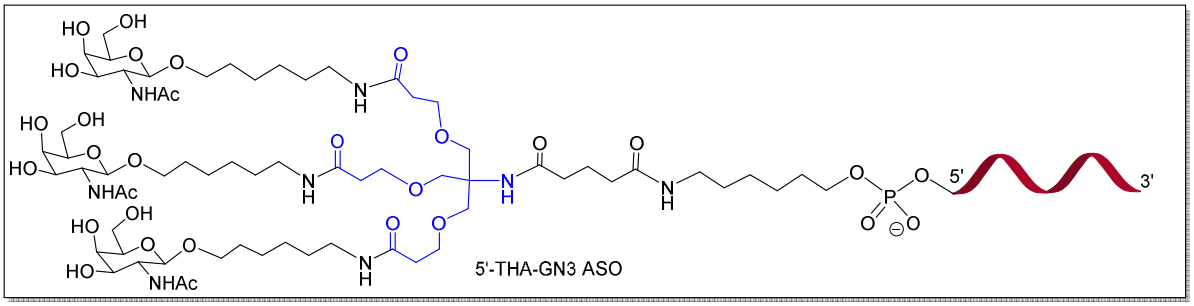

Figure 9. Structure of 5'-THA-GN3 ASO

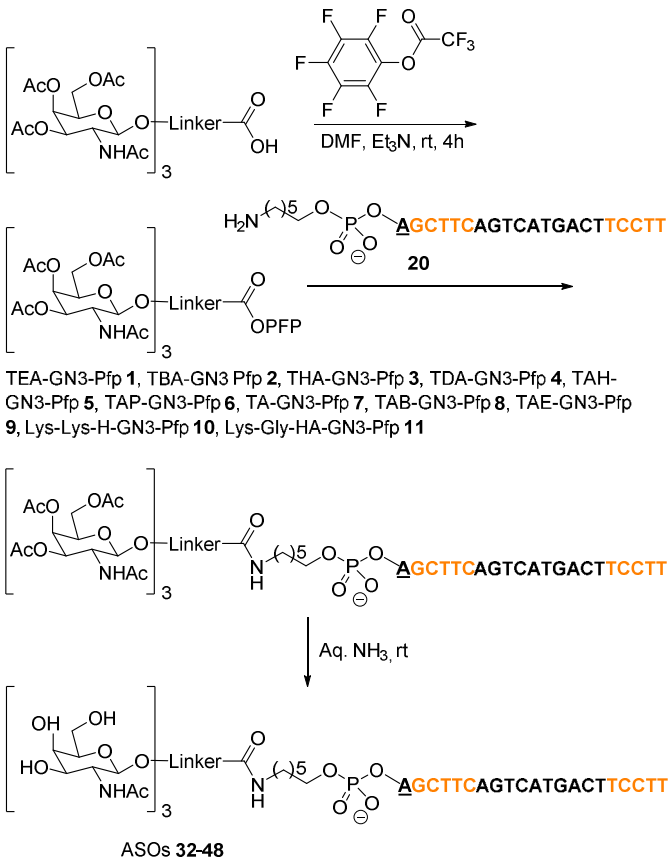

Scheme 1: Synthesis of GN3-Pfp esters **1-11** and 5'-GalNAc ASO conjugates **32-48**; All cytosine nucleobases are 5-methyl substituted, Orange letters indicate MOE nucleotides while black letters indicate DNA; All internucleosidic linkages were phosphoprothioate modified except for the underlined 5'-dA linker moiety which was phosphodiester linked.

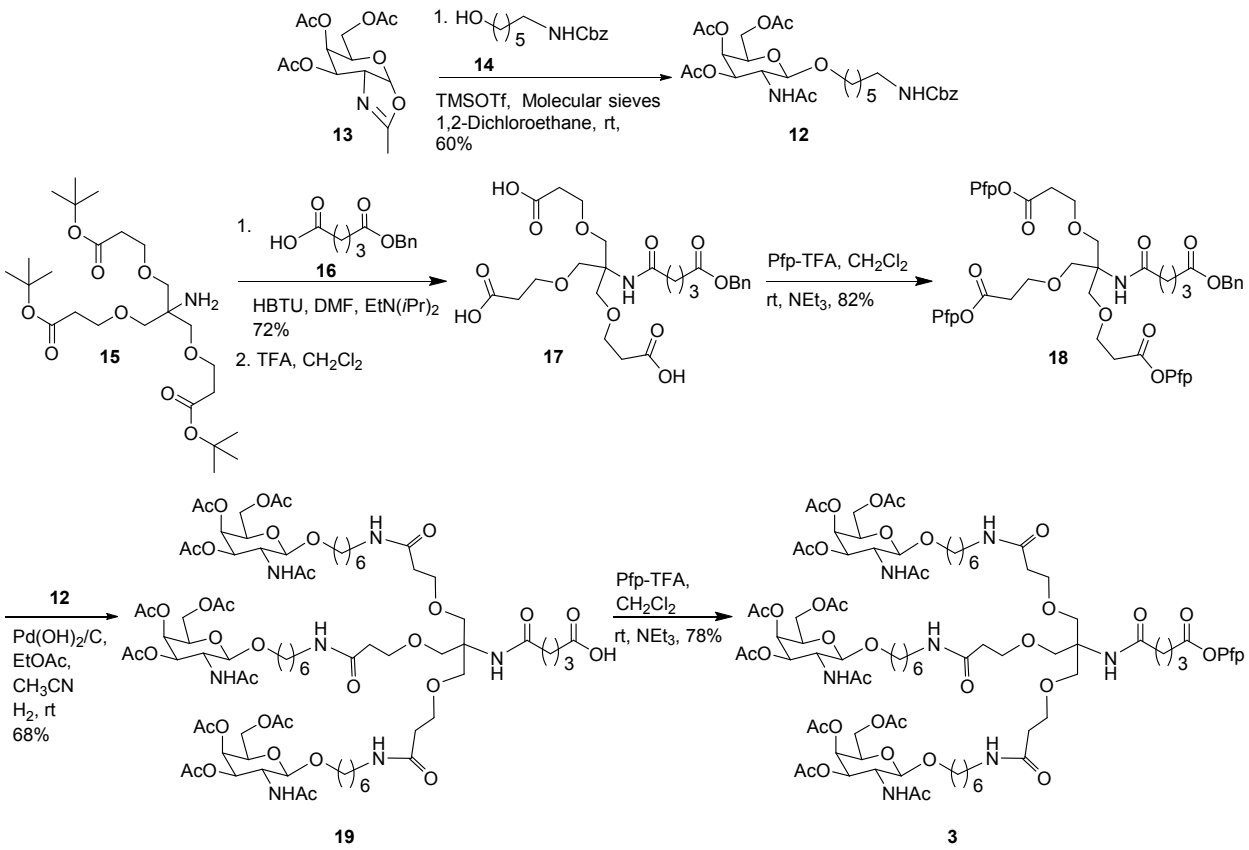

Scheme 2. Synthesis of THA-GN3-Pfp **3;** Pfp: pentafluorophenyl

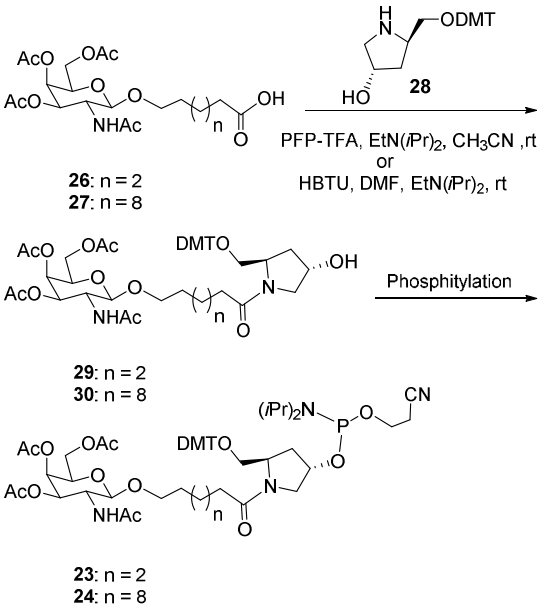

Scheme 3. Synthesis of hydroxyprolinol-GalNAc phosphoramidites **23-24**

"Table of Contents graphic"

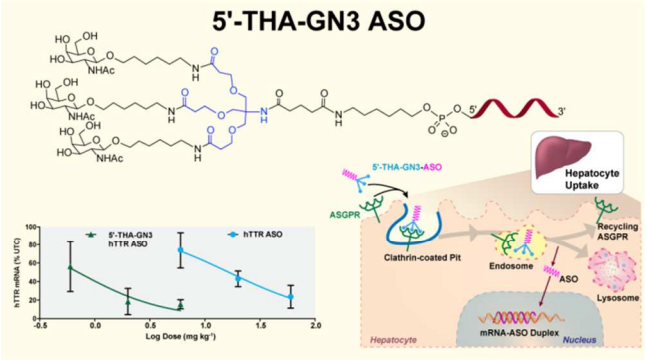

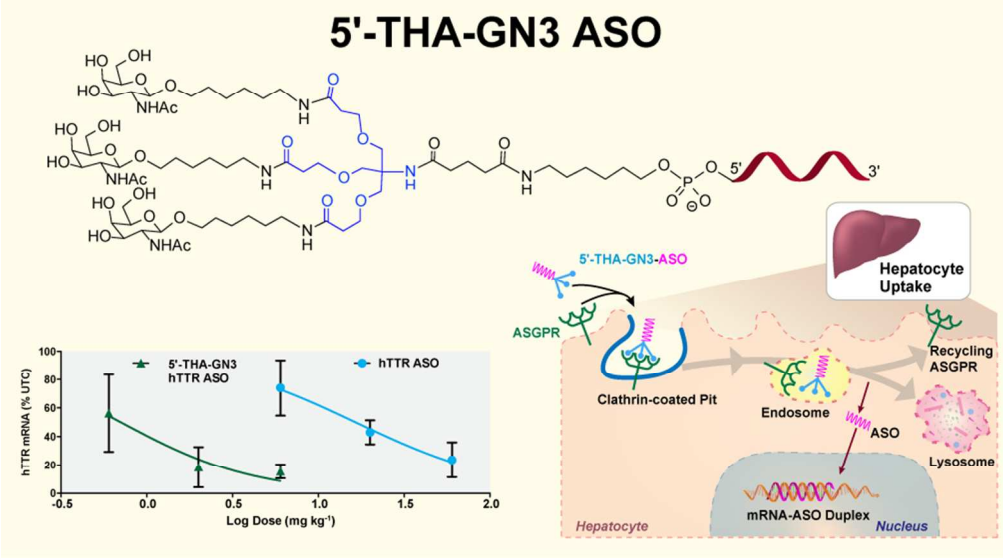

Table of Contents Graphic
85x47mm (300 x 300 DPI)